

## Lenses: Basic Optics

**Summary.** Basic optical formulae are derived, the transfer matrix method is explained, the lens action of apertures is shown, and emission, immersion and einzel lenses are treated.

A lens is characterized by the property that it imparts to a ray (particle trajectory) passing through it a deflection ( $\Delta r'$ ) which is proportional to the distance  $r_1$  from the axis, at which the ray passes, but which is independent of the original slope  $r'_1$ . For thin lenses this deflection may be assumed to be a sharp kink, occurring at the single principal plane  $P$ . If the entrance side – left of  $P$  – is designated by the index 1, and the exit side – right of  $P$  – by the index 2, one can write that the exit distance  $r_2$  equals the entrance distance  $r_1$  (Fig. 1.1):

$$r_1 = r_2, \quad (1.1)$$

and the exit slope  $r'_2$  equals the entrance slope  $r'_1$  plus the (negative) change of slope  $\Delta r'$ :

$$r'_2 = r'_1 + \Delta r'. \quad (1.2)$$

As stated above,  $-\Delta r' = cr_1$ , where  $c$  is the proportionality constant. It can be derived from the special case that the exit ray is parallel to the axis:

$$r'_2 = 0, \quad r'_1 = -\Delta r' = cr_1, \quad (1.3)$$

$$c = \frac{-\Delta r'}{r_1} = \frac{1}{f_1}. \quad (1.4)$$

In this case (Fig. 1.2) the entrance ray crosses the axis at the distance  $f_1$  from  $P$ ;  $f_1$  is the entrance focal length of the lens,  $F_1$  the entrance focal plane. Equation (1.2) can now be written as

$$r'_2 = r'_1 - \frac{r_1}{f_1}. \quad (1.5)$$

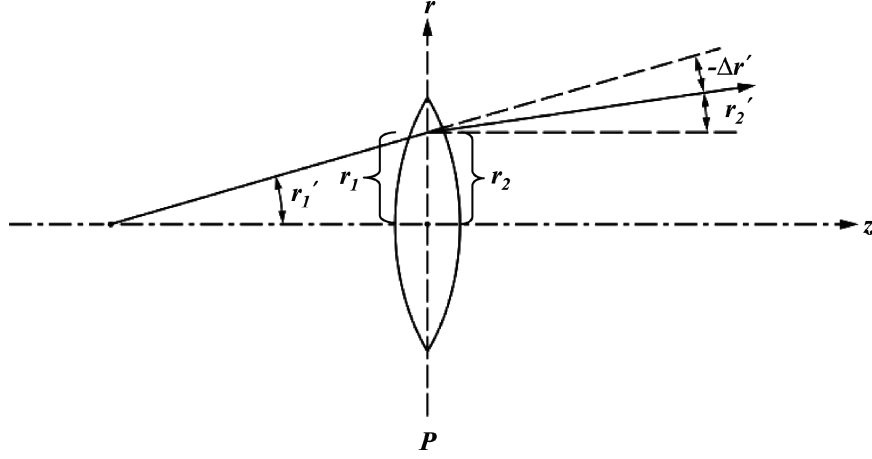


**Fig. 1.1.** Principle of a lens: A trajectory crossing the lens at distance  $r_1$  from the  $z$ -axis is deflected by an angle  $\Delta r'$  which is proportional to  $r_1$

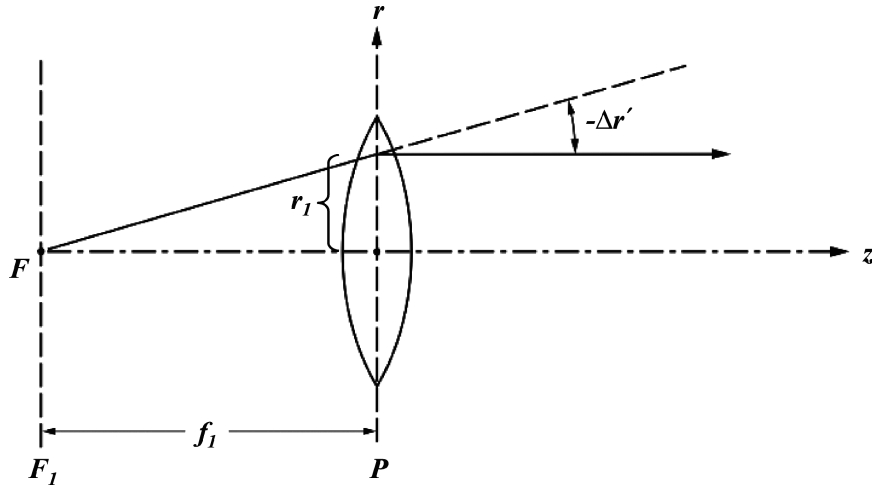


**Fig. 1.2.** Trajectories starting from the axis point  $F$  – the focal point – leave the lens parallel to the  $z$ -axis. The distance of the focal plane  $F_1$  to the lens plane  $P$  is the focal length  $f_1$

Equations (1.1) and (1.5) can be written in matrix form

$$\begin{pmatrix} r \\ r' \end{pmatrix}_2 = \begin{pmatrix} 1 & 0 \\ -\frac{1}{f_1} & 1 \end{pmatrix} \begin{pmatrix} r \\ r' \end{pmatrix}_1 = M_L \begin{pmatrix} r \\ r' \end{pmatrix}_1, \quad (1.6)$$

$M_L$  is called the transfer matrix of the lens.

The transfer matrix is

$$M_L = \begin{pmatrix} a_{11} & a_{12} \\ a_{21} & a_{22} \end{pmatrix}$$

with the coefficients

$$\begin{aligned} a_{11} &= 1, \\ a_{12} &= 0, \\ a_{21} &= -1/f_1, \\ a_{22} &= 1. \end{aligned}$$

In explicit form one has

$$\begin{aligned} r_2 &= a_{11}r_1 + a_{12}r'_1, \\ r'_2 &= a_{21}r_1 + a_{22}r'_1. \end{aligned}$$

This, with the above coefficients for a lens, yields (1.1) and (1.5).

Another way of describing the action of a lens is in the form of the exit equation of the ray in the  $z$ - $r$  coordinate system (Fig. 1.3):

$$r = ar'_1 + zr'_2 = ar'_1 + z \left( r'_1 - \frac{r_1}{f_1} \right),$$

where  $a$  is the distance of the object point  $A$  from  $P$ . With  $r_1 = ar'_1$  we have

$$r = \left[ a + z \left( 1 - \frac{a}{f_1} \right) \right] r'_1. \quad (1.7)$$

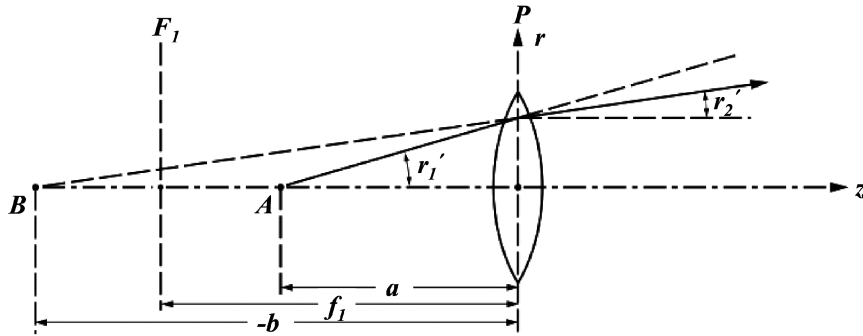


**Fig. 1.3.** The object point  $A$  is imaged to a virtual image point  $B$  if  $a < f_1$

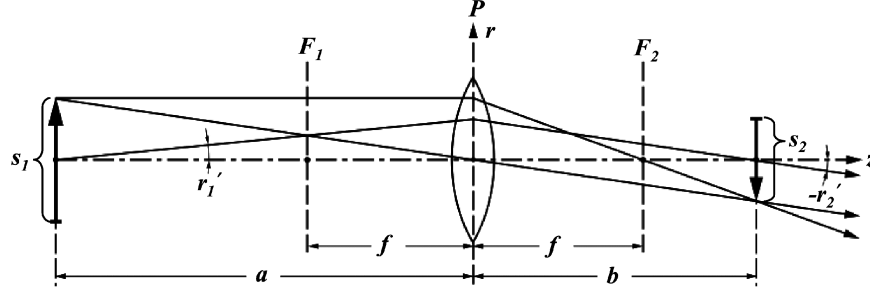


**Fig. 1.4.** Imaging of an extended object through a lens to a real image

The distance of the image point  $B$  – the point where the exit ray crosses the axis – from  $P$ , i.e. the image distance  $b$ , is obtained from (1.7) with  $r = 0$ :

$$a + b \left( 1 - \frac{a}{f_1} \right) = 0.$$

By dividing it by  $ab$ , this yields the familiar lens equation

$$\frac{1}{a} + \frac{1}{b} = \frac{1}{f_1}. \quad (1.8)$$

For  $a < f_1$ , as in Fig. 1.3, the image distance  $b$  is negative, i.e. the image is virtual.

For lenses, where the particle energy is the same on both the entrance and exit side, the focal lengths are also the same on both sides:

$$f_2 = f_1 = f. \quad (1.9)$$

For the imaging of an extended object (Fig. 1.4) the same rules apply as in light optics:

$$\text{lateral magnification: } M = \frac{s_2}{s_1} = \frac{b}{a}, \quad (1.10)$$

$$\text{angular magnification: } \frac{r'_2}{r'_1} = \frac{1}{M}. \quad (1.11)$$

Electrostatic lenses are generally thick lenses which have two principal planes  $P_1$  and  $P_2$ , and these are usually interchanged as shown in Fig. 1.5.

## 1.1 Simple Transfer Matrices

The transfer matrix of a lens has been introduced above. Transfer matrices become very useful when composite optical systems consisting

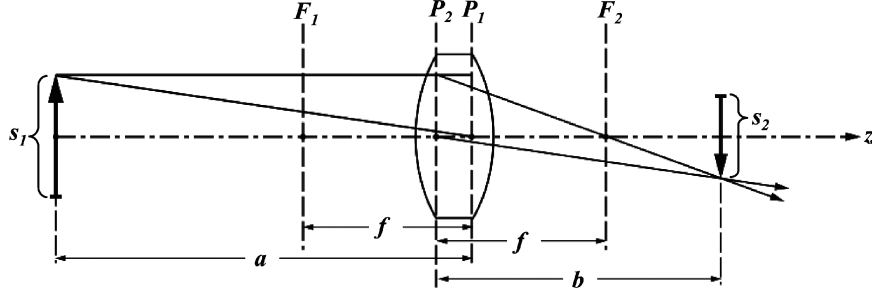


**Fig. 1.5.** Schematic of electrostatic lens with interchanged principal planes  $P_1$  and  $P_2$

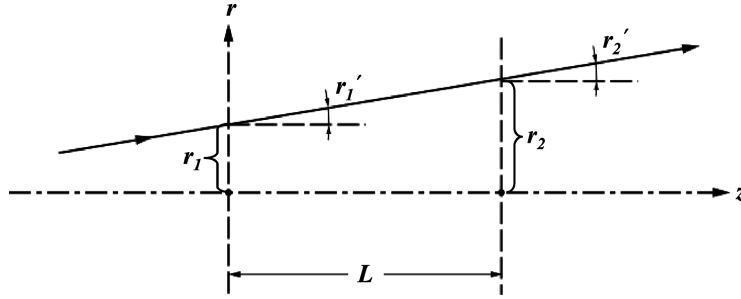


**Fig. 1.6.** Drift space without deflection

of several elements in tandem are to be treated. Frequently, just one property of the composite system is of interest, e.g. the magnification, and therefore only one of the matrix coefficients needs to be calculated, which can often be done very quickly with the aid of a hand calculator. The simplest transfer matrix is that of a drift space (Fig. 1.6).

From the figure one can see immediately that

$$r_2 = r_1 + L r_1', \quad (1.12)$$

$$r_2' = r_1', \quad (1.13)$$

or in transfer matrix form

$$\begin{pmatrix} r \\ r' \end{pmatrix}_2 = \begin{pmatrix} 1 & L \\ 0 & 1 \end{pmatrix} \begin{pmatrix} r \\ r' \end{pmatrix}_1 = M_D \begin{pmatrix} r \\ r' \end{pmatrix}_1. \quad (1.14)$$

When two optical elements are combined in tandem, their respective transfer matrices have to be multiplied. For the combination of a lens

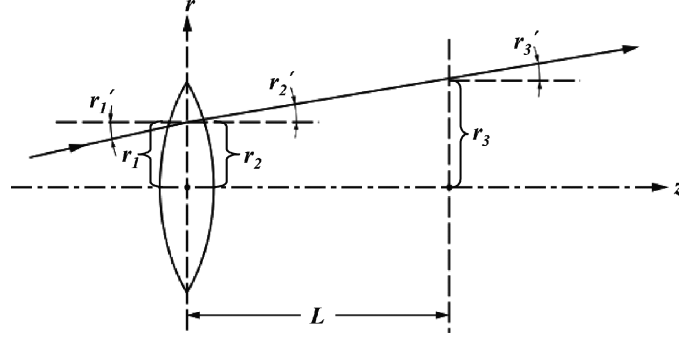


**Fig. 1.7.** Combination of einzel lens with drift space

and a drift space (Fig. 1.7) one has therefore to multiply the transfer matrices of the lens and the drift space:

$$\begin{pmatrix} r \\ r' \end{pmatrix}_3 = \underbrace{\begin{pmatrix} b_{11} & b_{12} \\ b_{21} & b_{22} \end{pmatrix}}_{\text{drift space}} \begin{pmatrix} r \\ r' \end{pmatrix}_2 = \underbrace{\begin{pmatrix} b_{11} & b_{12} \\ b_{21} & b_{22} \end{pmatrix}}_{\text{drift space}} \underbrace{\begin{pmatrix} a_{11} & a_{12} \\ a_{21} & a_{22} \end{pmatrix}}_{\text{lens}} \begin{pmatrix} r \\ r' \end{pmatrix}_1, \quad (1.15)$$

$$\begin{pmatrix} r \\ r' \end{pmatrix}_3 = \begin{pmatrix} c_{11} & c_{12} \\ c_{21} & c_{22} \end{pmatrix} \begin{pmatrix} r \\ r' \end{pmatrix}_1.$$

The coefficients  $c_{ik}$  are found according to the scheme

$$c_{ik} = \sum_{s=1}^2 b_{is} a_{sk}, \quad i, k = 1, 2,$$

or explicitly

$$\begin{aligned} c_{11} &= b_{11}a_{11} + b_{12}a_{21}, \\ c_{12} &= b_{11}a_{12} + b_{12}a_{22}, \\ c_{21} &= b_{21}a_{11} + b_{22}a_{21}, \\ c_{22} &= b_{21}a_{12} + b_{22}a_{22}. \end{aligned}$$

In our example, we have with (1.14),

$$\begin{aligned} b_{11} &= 1, & b_{12} &= L, \\ b_{21} &= 0, & b_{22} &= 1. \end{aligned}$$

With these and the coefficients of the lens transfer matrix, one then obtains

$$\begin{aligned} c_{11} &= 1 - \frac{L}{f}, & c_{12} &= L, \\ c_{21} &= -\frac{1}{f}, & c_{22} &= 1. \end{aligned}$$

Explicitly, this reads

$$\begin{aligned} r_2 &= r_1 + L \left( r_1' - \frac{r_1}{f} \right), \\ r_2' &= r_1' - \frac{r_1}{f}. \end{aligned}$$

When the sequence of the two elements is reversed, i.e. drift space followed by lens, the  $a_{iks}$  and  $b_{iks}$  are interchanged. This yields

$$\begin{aligned} c_{11}^* &= a_{11}b_{11} + a_{12}b_{21}, \\ c_{12}^* &= a_{11}b_{12} + a_{12}b_{22}, \\ c_{21}^* &= a_{21}b_{11} + a_{22}b_{21}, \\ c_{22}^* &= a_{21}b_{12} + a_{22}b_{22}, \\ c_{11}^* &= 1, & c_{12}^* &= L, \\ c_{21}^* &= -\frac{1}{f}, & c_{22}^* &= 1 - \frac{L}{f}. \end{aligned}$$

## 1.2 Passage of Charged Particles Through a Uniform Electrostatic Field

Figure 1.8 shows the important case where a charged particle is accelerated through a uniform field between the equipotential planes denoted  $P_1$  and  $P_2$ . The spaces to the left of  $P_1$  and right of  $P_2$  are field free and have the potentials  $V_1$  and  $V_2$ . The potentials are counted from where the charged particles have zero energy so that their kinetic energy in flight direction at any point in space with the potential  $V_i$  is  $eV_i$ .

In this simple case the differential equations of motion can be straightforwardly integrated and yield the motion of the particle in the  $z$ - $r$ -coordinate system as a function of time  $t$ :

$$\begin{aligned} m\ddot{r} &= 0, & m\ddot{z} &= eE, & z_1 &= r_1 = 0, \\ \dot{z}_1 &= v_1 \cos \alpha_1, & \dot{r}_1 &= v_1 \sin \alpha_1, & v_1 &= \sqrt{2e\frac{V_1}{m}} \end{aligned}$$

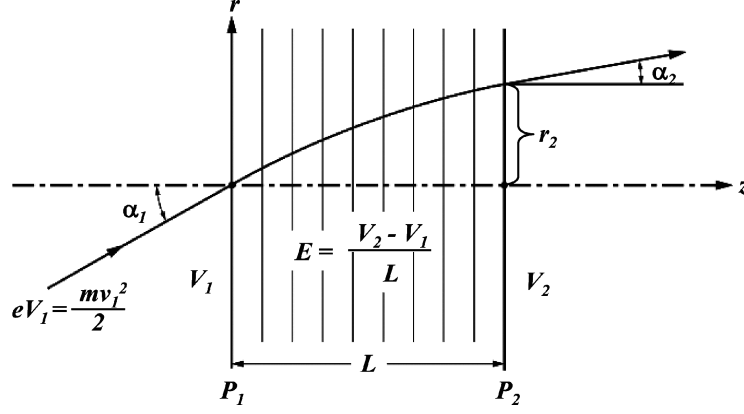


**Fig. 1.8.** Acceleration of charged particle through a uniform field

( $v_1$  is the velocity of the particle at energy  $eV_1$ ,  $m$  its mass).

$$\dot{z} = \frac{eE}{m}t + v_1 \cos \alpha_1, \quad z = \frac{eE}{2m}t^2 + v_1 \cos \alpha_1 \cdot t, \quad (1.16)$$

$$\dot{r} = \dot{r}_1 = v_1 \sin \alpha_1, \quad r = v_1 \sin \alpha_1 \cdot t. \quad (1.17)$$

By eliminating the time  $t$  one obtains the trajectory:

$$\begin{aligned} \frac{eE}{2mv_1}t^2 + \cos \alpha_1 \cdot t - \frac{z}{v_1} &= 0, \\ t &= \frac{mv_1}{eE} \left( \sqrt{\cos^2 \alpha_1 + \frac{2eE}{mv_1^2}z} - \cos \alpha_1 \right), \\ r &= \frac{2V_1}{E} \sin \alpha_1 \left( \sqrt{\frac{E}{V_1}z + \cos^2 \alpha_1} - \cos \alpha_1 \right). \end{aligned} \quad (1.18)$$

This is the equation of the trajectory within the field. At the end of the field where  $z = L$ , the distance from the  $z$ -axis is obtained with

$$\frac{E}{V_1} = \frac{1}{L} \left( \frac{V_2}{V_1} - 1 \right)$$

as

$$r_2 = \frac{2L \sin \alpha_1}{\frac{V_2}{V_1} - 1} \left( \sqrt{\frac{V_2}{V_1} - \sin^2 \alpha_1} - \cos \alpha_1 \right) \quad (1.19)$$



The slope of the trajectory at  $P_2$  is found by differentiating (1.18) with respect to  $z$  and setting  $z = L$ :

$$\begin{aligned} r' &= \frac{dr}{dz} = \sin \alpha_1 \left( \frac{E}{V_1} z + \cos^2 \alpha_1 \right)^{-1/2} \\ r'_2 &= \sin \alpha_1 \left( \frac{V_2}{V_1} - \sin^2 \alpha_1 \right)^{-1/2}. \end{aligned} \quad (1.20)$$

From (1.20) the refractive index for charged particles can be derived: rewriting  $r'_2$  one obtains

$$r'_2 = \tan \alpha_2 = \frac{\sin \alpha_2}{\sqrt{1 - \sin^2 \alpha_2}},$$

and putting this into (1.20) yields

$$\begin{aligned} \frac{\sin \alpha_2}{\sqrt{1 - \sin^2 \alpha_2}} &= \frac{\sin \alpha_1}{\sqrt{\frac{V_2}{V_1} - \sin^2 \alpha_1}}, \\ \frac{V_2}{V_1} - \sin^2 \alpha_1 &= \frac{\sin^2 \alpha_1}{\sin^2 \alpha_2} (1 - \sin^2 \alpha_2) = \frac{\sin^2 \alpha_1}{\sin^2 \alpha_2} - \sin^2 \alpha_1, \end{aligned}$$

and finally

$$\frac{\sin \alpha_2}{\sin \alpha_1} = \sqrt{\frac{V_1}{V_2}}. \quad (1.21)$$

Note that the distance  $L$  does not appear in (1.21).

If one could compress the field to an infinitely narrow double-layer with the potentials  $V_1$  and  $V_2$  on either side, one would have the exact analogue to the refraction of light at the interface between two media with the refractive indices  $n_1$  and  $n_2$  (Fig. 1.9), where the familiar law of refraction is valid. Comparing this with (1.21) reveals that in electrostatic optics the square root of the potential plays the role of the refractive index  $n$ , the difference being that in light optics sharp interfaces are the rule, while in particle optics one has gradual transitions of the refractive index. (An example in light optics would be radially graded fibers in fiber optics.) Another difference of practical significance is that in electrostatic optics the particle energy and with its square root the refractive index can vary over many orders of magnitude, while the variation of the refractive index of transparent substances stays within half an order of magnitude.

The above equations are valid not only for acceleration ( $V_2 > V_1$ ), but also for deceleration ( $V_2 < V_1$ ). In the latter case, the expression

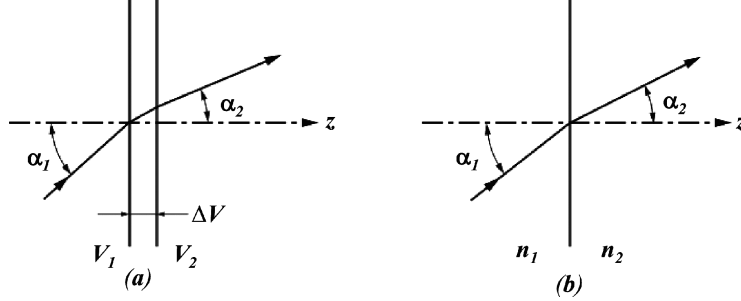


**Fig. 1.9.** Refraction of charged particle trajectories (a) compared to that of light (b)

under the square root of (1.19) and (1.20) may become negative, when  $V_2/V_1 < \sin^2 \alpha_1$ , and the exit ordinate  $r_2$  becomes imaginary. The physical meaning of this is that the particle does not reach the exit plane  $P_2$  but is reflected before it. This case can be treated by expressing the abscissa  $z$  of the flying particle as a function of the ordinate  $r$ ; i.e. by reversing (1.18).

One can obtain this directly by substituting the time  $t$  in (1.16) by  $t$  from (1.17). The result is

$$z = \frac{E}{4V_1} \frac{r^2}{\sin^2 \alpha_1} + \frac{r}{\tan \alpha_1}. \quad (1.22)$$

This is the equation of the parabolic trajectory shown in Fig. 1.10 of the particle reflected in the decelerating field. Differentiating this equation with respect to  $r$  yields the slope against the  $r$ -ordinate:

$$\frac{dz}{dr} = \frac{E}{2V_1} \frac{r}{\sin^2 \alpha_1} + \frac{1}{\tan \alpha_1}. \quad (1.23)$$

The turning point of the parabola ( $z_{\max}, r_m$ ) is found by setting (1.23) equal to zero:

$$r_m = -2 \frac{V_1}{E} \sin \alpha_1 \cos \alpha_1, \quad (1.24)$$

$$z_{\max} = \frac{E}{4V_1} \frac{r_m^2}{\sin^2 \alpha_1} + \frac{r_m}{\tan \alpha_1} = -\frac{V_1}{E} \cos^2 \alpha_1. \quad (1.25)$$

(The minus sign of these expressions is cancelled by the negative  $E$ , see Fig. 1.10.)

For symmetry reasons, the distance of the point where the particle leaves the field again is  $2r_m$  apart from the point of entrance.

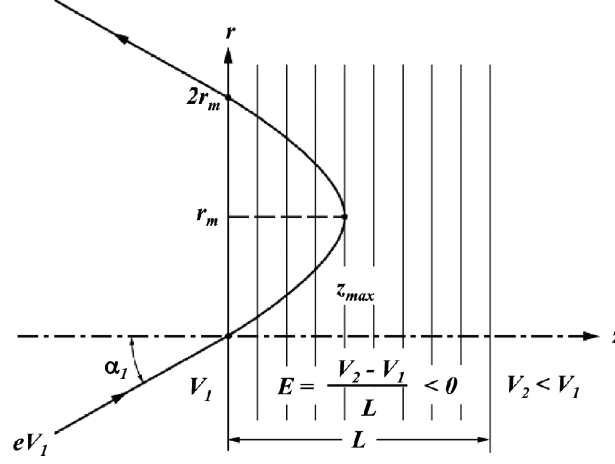


Fig. 1.10. Reflection of charged particle by a decelerating field

In the special case  $\alpha_1 = 45^\circ$  one obtains

$$r_m = -\frac{V_1}{E}, \quad z_{\max} = -\frac{V_1}{2E} = \frac{r_m}{2}.$$

The point of exit in this case is four times  $z_{\max}$  apart from the point of entrance ( $2r_m = 4z_{\max}$ ).

It so happens that in this special case,  $\alpha_1 = 45^\circ$ ,  $r_m$  and therefore  $2r_m$  have a maximum. This is derived easily by differentiating  $r_m$  with respect to  $\alpha_1$  and setting the result equal to zero:

$$\frac{\partial r_m}{\partial \alpha_1} = -2\frac{V_1}{E} (\cos^2 \alpha_1 - \sin^2 \alpha_1) = 0, \quad \alpha_1 = 45^\circ.$$

This means also that the trajectories which have slightly different entrance angle variations  $\Delta\alpha_1$  around  $\alpha_1 = 45^\circ$  (Fig. 1.11) cross each other and the trajectory with  $\alpha_1 = 45^\circ$  at the distance  $2r_m$ . In other words, the retarding field has focusing properties.

It forms a first-order image of the entrance point at the exit point. This happens of course only two-dimensionally, viz. in the drawing plane. The abscissa of the turning point is found by differentiating  $z_{\max}$ , (1.25), with respect to  $\alpha_1$ :

$$\frac{\partial z_{\max}}{\partial \alpha_1} = 2\frac{V_1}{E} \sin \alpha_1 \cos \alpha_1, \quad \text{and with } \alpha_1 = 45^\circ, \Delta z_{\max} = \frac{V_1}{E} \Delta \alpha_1.$$

Another property of the electrostatic field can be demonstrated here, i.e. energy dispersion. When  $r_m$  is differentiated with respect to the

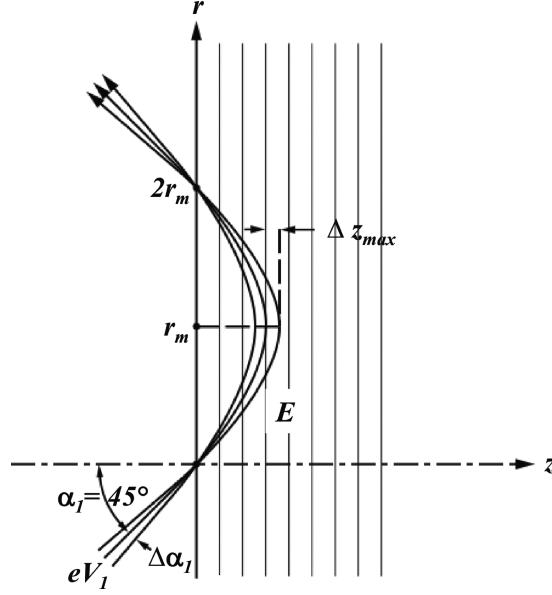


Fig. 1.11. Focusing properties of decelerating field

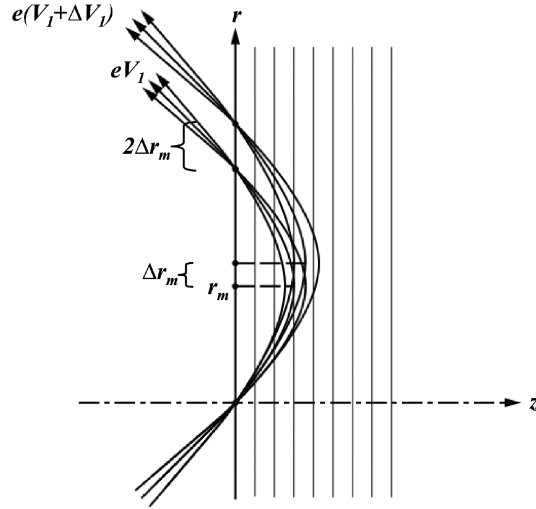


Fig. 1.12. Energy dispersion of decelerating field

particle energy  $eV_l$  one obtains from (1.24) (Fig. 1.12)

$$\frac{\partial r_m}{\partial V_l} = -\frac{2}{E} \sin \alpha_l \cos \alpha_l, \text{ and with } \alpha_l = 45^\circ, \quad 2\Delta r_m = -\frac{2}{E} \Delta V_l. \quad (1.26)$$

The variation of  $z_{\max}$  is found by differentiating it with respect to  $V_1$  (1.25):

$$\frac{\partial z_{\max}}{\partial V_1} = -\frac{\cos^2 \alpha_1}{E}, \text{ and with } \alpha_1 = 45^\circ, \Delta z_{\max} = -\frac{1}{2E} \Delta V_1 = \frac{\Delta r_m}{2}.$$

The uniform electrostatic field is a simple yet instructive example to demonstrate the focusing and dispersive properties of an electrostatic field, which can be derived in a few lines from first principles. In the examples to follow the derivation will not be presented but was found by the same means.

### 1.3 Transfer Matrix of the Uniform Field

Equations (1.19) and (1.20) represent a rigorous description of the trajectory's exit ordinate and slope after passage through a uniform field. When considering the paraxial case ( $\alpha_1 \ll 1$ , Fig. 1.13) one obtains the simpler expressions, with  $\sin \alpha_1 \approx r'_1$ ,  $\cos \alpha_1 \approx 1$ ,  $r'_1 \ll V_2/V_1$ ,

$$r_2 \approx \frac{2Lr'_1}{\frac{V_2}{V_1} - 1} \left( \sqrt{\frac{V_2}{V_1}} - 1 \right) = \frac{2L}{\sqrt{\frac{V_2}{V_1}} + 1} r'_1, \quad (1.27)$$

$$r'_2 \approx \sqrt{\frac{V_1}{V_2}} r'_1, \quad (1.28)$$

In the general case, with  $r_1 \neq 0$ , one has therefore

$$r_2 = r_1 + \frac{2L}{\sqrt{\frac{V_2}{V_1}} + 1} r'_1,$$

$$r'_2 = \sqrt{\frac{V_1}{V_2}} r'_1,$$

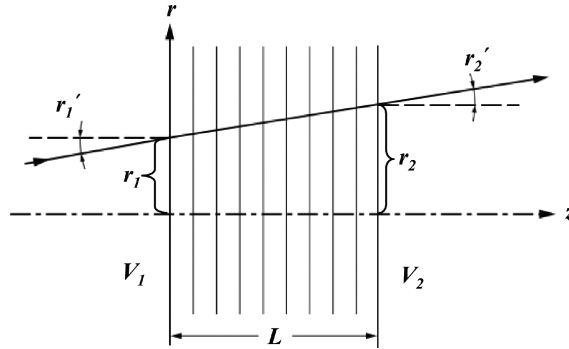


Fig. 1.13. Paraxial case of acceleration of charged particle through a uniform field

or in matrix form

$$\begin{pmatrix} r \\ r' \end{pmatrix}_2 = \begin{pmatrix} 1 & \frac{2L}{\sqrt{V_1/V_2+1}} \\ 0 & \sqrt{V_1/V_2} \end{pmatrix} \begin{pmatrix} r \\ r' \end{pmatrix}_1 = M_F \begin{pmatrix} r \\ r' \end{pmatrix}_1.$$

The transfer matrix coefficients of the uniform electrostatic field are thus

$$\begin{aligned} a_{11} &= 1, & a_{12} &= \frac{2L}{1 + \sqrt{\frac{V_2}{V_1}}}, \\ a_{21} &= 0, & a_{22} &= \sqrt{\frac{V_1}{V_2}}. \end{aligned}$$

This is valid not only for acceleration ( $V_2/V_1 > 1$ ), but also for deceleration ( $V_2/V_1 < 1$ ). For the case of mere drift ( $V_2/V_1 = 1$ ) the matrix coefficients for a drift space (1.14) result.

#### 1.4 Acceleration of Charged Particles Emitted from a Planar Surface

A special case of practical importance is the acceleration of charged particles emitted or reflected from a planar conducting surface (Fig. 1.14).

When a charged particle leaves the surface with energy  $eV_1$  and is accelerated by the voltage  $V_a$  it will leave the uniform acceleration field with energy  $e(V_1 + V_a)$ . With this definition, (1.19) and (1.20) now read, since  $V_2 = V_1 + V_a$ ,

$$r_2 = 2L \frac{V_1}{V_a} \sin \alpha_1 \left( \sqrt{\frac{V_a}{V_1} + \cos^2 \alpha_1} - \cos \alpha_1 \right), \quad (1.29)$$

$$r'_2 = \sin \alpha_1 \left( \frac{V_a}{V_1} + \cos^2 \alpha_1 \right)^{-1/2}. \quad (1.30)$$

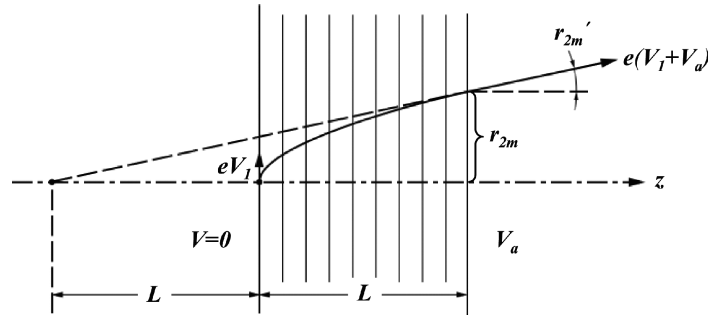


**Fig. 1.14.** Acceleration of charged particles emitted from planar conducting surface

For particles leaving the surface at a glancing angle ( $\alpha_1 = 90^\circ$ ) the maximum values of  $r_2$  and  $r'_2$  are obtained:

$$r_{2m} = 2L\sqrt{\frac{V_1}{V_a}}, \quad (1.31)$$

$$r'_{2m} = \sqrt{\frac{V_1}{V_a}}. \quad (1.32)$$

The virtual starting point of these particles is located at the distance  $r_{2m}/r'_{2m} = 2L$  behind the end of the uniform field, i.e. at the distance  $L$  behind the surface. This holds exactly for any positive value of  $V_1/V_a$ .

In most practical cases the acceleration voltage  $V_a$  is large in comparison to the starting voltage  $V_1$ . With this condition (1.29) and (1.30) become

$$r_2 \approx 2L\sqrt{\frac{V_1}{V_a}}\sin\alpha_1, \quad (1.33)$$

$$r'_2 \approx \sqrt{\frac{V_1}{V_a}}\sin\alpha_1. \quad (1.34)$$

The virtual starting point is found as above by forming  $r_2/r'_2$ . Since  $\alpha_1$  cancels out, the virtual starting point is now also located at the distance  $L$  behind the surface for any starting angle, but only in first approximation for  $V_a \gg V_1$  (Fig. 1.15).

After the acceleration the trajectories are paraxial ( $r'_2 \ll 1$ ). An extended emitting surface element of dimension  $D_1$  is imaged to a virtual surface element of dimension  $D_2 = D_1$ , i.e. the magnification is unity.

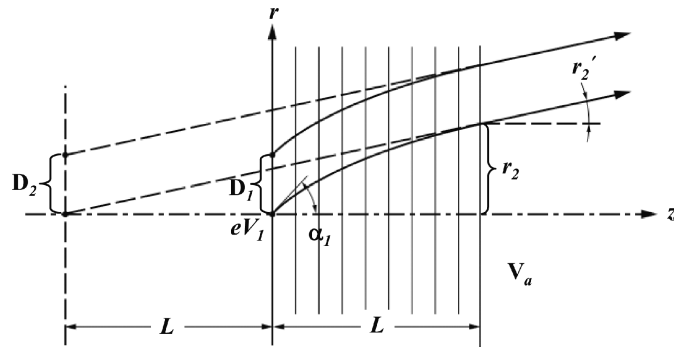


**Fig. 1.15.** Virtual imaging of surface emitting charged particles by accelerating field

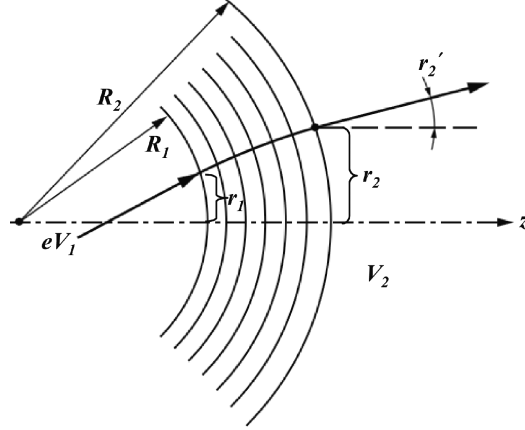


**Fig. 1.16.** Electrostatic field between concentric spherical equipotential surfaces

### 1.5 Transfer Matrix of Electrostatic Field Between Spherical Concentric Equipotential Surfaces

The case of charged particles passing through a field between concentric spherical equipotential surfaces with the radii  $R_1$  and  $R_2$  (Fig. 1.16) has also some practical importance, particularly for electron or ion sources [1]. The paraxial transfer matrix is therefore presented here, but without derivation [2]:

$$\begin{pmatrix} r \\ r' \end{pmatrix}_2 = \begin{pmatrix} \frac{R_2}{R_1} (1 - k_1) & R_2 k_1 \\ \frac{1}{R_1} (1 - k_1 - k_2) & k_1 + k_2 \end{pmatrix} \begin{pmatrix} r \\ r' \end{pmatrix}_1$$

with the abbreviations

$$k_1 = 2 \frac{1 - R_1/R_2}{1 + \sqrt{V_2/V_1}} \quad \text{and} \quad k_2 = \frac{R_1}{R_2} \sqrt{\frac{V_1}{V_2}}.$$

This is also valid for acceleration ( $V_2/V_1 > 1$ ), drift ( $V_2/V_1 = 1$ ) or deceleration ( $V_2/V_1 < 1$ ). From the above matrix coefficients those of the uniform field can be derived by performing the transitions  $R_1, R_2 \rightarrow \infty$  and  $R_2 - R_1 = L$ .

### 1.6 Acceleration of Charged Particles Emitted from a Spherical Surface

A practical example of acceleration of charged particles from a spherical surface are tip sources of electrons or ions (Fig. 1.17). In these cases



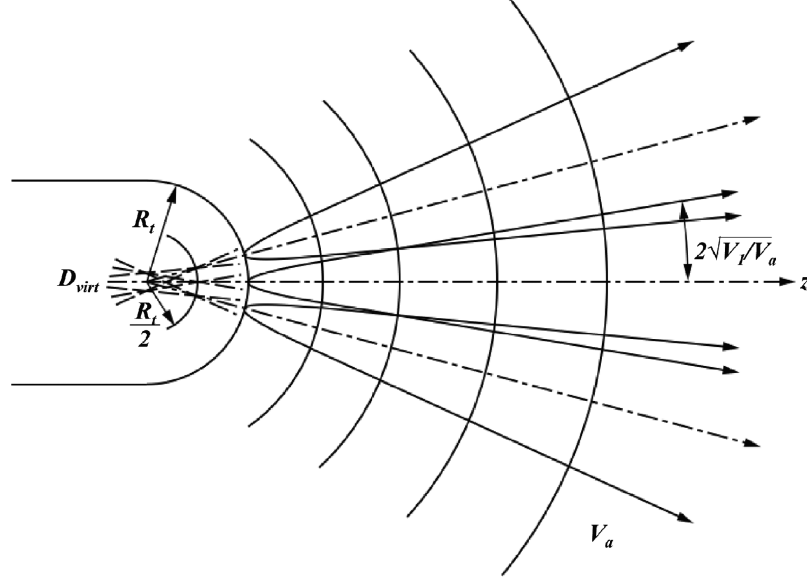


**Fig. 1.17.** Acceleration of charged particles between concentric spherical emitting and accelerating equipotential surfaces

the acceleration energy  $eV_a$  is usually large in comparison to the initial energy  $eV_1$ .

Furthermore, the tip radius  $R_t$  is small in comparison to the distance of the acceleration electrode, the shape of which is then unimportant because the main acceleration takes place within a distance of a few tip radii in the field determined solely by the tip. Under these conditions, the trajectories of particles starting at a glancing angle from the surface have after acceleration by  $V_a$  a slope of  $2\sqrt{V_1/V_a}$  against the surface normal, as compared to  $\sqrt{V_1/V_a}$  in the planar case (comp. (1.32)), and the virtual starting point lies at the distance  $R_t/2$  behind the emitting surface. Thus, the emitting surface is imaged to a virtual surface having the radius  $R_t/2$ . But more significant is the fact that all trajectories with maximum slope  $2\sqrt{V_1/V_a}$  to the normal of their starting points, when extended backwards to the center of the semi-sphere, have a distance of  $\frac{R_t}{2} 2\sqrt{\frac{V_1}{V_a}} = R_t \sqrt{\frac{V_1}{V_a}}$  from the center. Therefore, this appears as the virtual source radius. In this way, microsources can be realized by simple means. For example thermionically emitted particles have initial energies of less than 1 eV, so with an acceleration voltage of 10 kV the virtual source radius is 100 times smaller than the tip radius. All of this is of course valid only when the acceleration voltage is not

screened by a Wehnelt electrode, which would drastically alter the field around the tip.

### 1.7 Passage of Charged Particles Through an Electrode with Round Aperture

In practice, an acceleration field such as shown in Fig. 1.15 is terminated by a planar electrode with an aperture centered to the axis for passage of the accelerated particles (Fig. 1.18). This aperture causes the equipotential surfaces to bulge through it towards the field-free space.

When the field strength is considered near the hole, one sees that a radial component  $E_r$  is present acting so as to deflect the particles away from the axis.

It can be shown that this round opening acts as a lens [3]: We place a fictitious cylinder axially through the hole so that its left end protrudes to the region of the undisturbed uniform field, while its right end reaches into the field free space. From the conservation of field line flux we obtain, there being no space charge,

$$r^2 \pi E_a + 2r \pi \int_{-a}^{+b} E_r dz = 0, \quad r E_a + 2 \int_{-a}^{+b} E_r dz = 0. \quad (1.35)$$

A charged particle passing from the left at the distance  $r$  from the axis experiences a radial momentum:

$$mv_r = - \int e E_r dt = - \frac{e}{v_z} \int_{-a}^{+b} E_r dz, \quad (1.36)$$

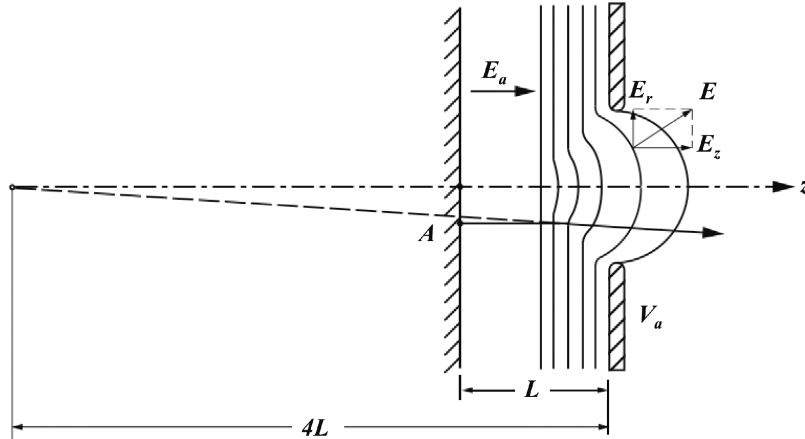


**Fig. 1.18.** Diverging action of aperture terminating an acceleration field

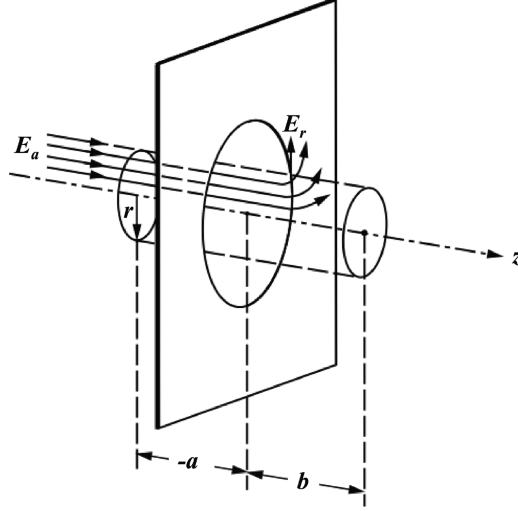


**Fig. 1.19.** Derivation of lens action of an aperture terminating an acceleration field

whereby  $v_z = dz/dt$ ,  $dt = dz/v_z$  was substituted. Since the trajectory is paraxial,  $v_z$  can be considered constant. Substituting the integral from (1.35) we obtain

$$mv_r = \frac{er}{2v_z} E_a. \quad (1.37)$$

The trajectory suffers a kink  $\Delta r'$  (Fig. 1.20) given by, with (1.37),  $\Delta r' = v_r/v_z = erE_a/2mv_z^2$ . With  $mv_z^2/2 = eV$ , the particle energy, we then obtain

$$\Delta r' = \frac{E_a}{4V} r.$$

The trajectory deflection  $\Delta r'$  thus is proportional to the distance from the axis. This is the characterization of a lens. The focal length is given by (comp. (1.4))

$$-f = \frac{r}{\Delta r'} = \frac{4V}{E_a}. \quad (1.38)$$

As in most practical cases the acceleration energy  $eV_a$  is large in comparison with the initial particle energy, one can replace the particle energy at the aperture  $eV$  by  $eV_a$ , and thus  $E_a = V_a/L$  (see Fig. 1.18). This yields

$$-f = 4L \quad (1.39)$$

The aperture acts as a diverging lens with the focal length  $-4L$  [4].

A particle starting off-axis from point  $A$  normal to the surface appears to have started on the axis at a distance of  $3L$  behind the emitting surface (Fig. 1.18). The virtual surface located at the distance  $L$

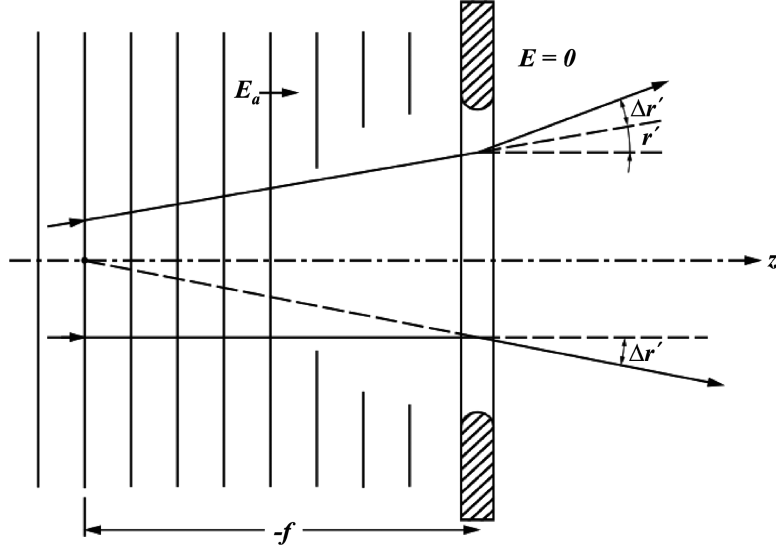


Fig. 1.20. Deflection of trajectories passing through the aperture

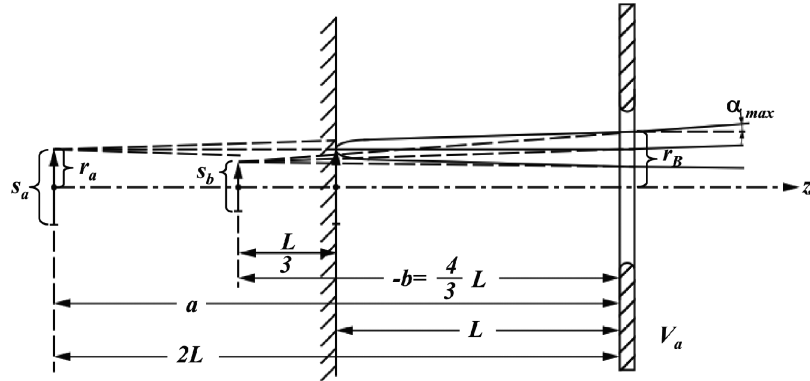


Fig. 1.21. Imaging of emitting surface by accelerating field and aperture

behind the emitting surface (Figs. 1.15 and 1.21) is imaged to a distance of  $4/3L$  to the left of the aperture, i.e. to a distance of  $L/3$  behind the emitting surface.

This can easily be derived geometrically (see Fig. 1.21) or by calculation with the lens formula (1.8):

$$\frac{1}{b} = -\frac{1}{4L} - \frac{1}{2L} = -\frac{3}{4L} \quad , \quad b = -\frac{4}{3}L.$$

The magnification is  $s_b/s_a = \frac{4}{3}L/2L = 2/3$ .

For particles with initial energy  $eV_1$ , the beam radius at the aperture is with (1.31),  $r_B = r_a + 2L\sqrt{V_1/V_a}$  and the maximum beam angle  $\alpha_{\max}$  after passage through the aperture is, with (1.32) and (1.39),

$$\alpha_{\max} = \sqrt{\frac{V_1}{V_a}} + \frac{r_B}{4L}.$$

These values are important to know when designing acceleration optics without obstructing parts of the beam by electrodes.

The combination: uniform field followed by an aperture, can be treated very simply and conveniently by forming the product of the transfer matrices for the uniform field with that for a lens (1.6):

$$\begin{aligned} M_F M_L &\equiv \begin{pmatrix} 1 & \frac{2L}{\sqrt{V_2/V_1+1}} \\ 0 & \sqrt{V_1/V_2} \end{pmatrix} \begin{pmatrix} 1 & 0 \\ -\frac{1}{f_2} & 1 \end{pmatrix} \\ &= \begin{pmatrix} 1 & \frac{2L}{\sqrt{V_2/V_1+1}} \\ -\frac{1}{f_2} & -\frac{1}{f_2} \frac{2L}{\sqrt{V_2/V_1+1}} + \sqrt{\frac{V_1}{V_2}} \end{pmatrix} \equiv M_{FL}. \end{aligned}$$

The focal length  $f_2$  is that of the aperture according to (1.39).

## 1.8 General Aperture

Equation (1.39) is just a special case of the general formula for the lens effect of an aperture separating two regions of different field strengths (Fig. 1.22) [4]:

$$f = \frac{4V_a}{E_2 - E_1}, \quad (1.40)$$

where  $V_a$  is the voltage of the aperture (particle energy =  $eV_a$ ) measured against the particle source (zero particle energy), and  $E_1$  and  $E_2$  are the field strengths on both sides of the aperture. The signs of the field strengths are defined such that a positive field strength accelerates and a negative field strength decelerates. Thus for  $E_1 > E_2$  the focal length is negative, meaning a diverging lens (as in the case above, where  $E_2 = 0$ ), while for  $E_1 < E_2$  the aperture acts as a converging lens,  $f$  being positive.

Various cases are possible, shown schematically in Fig. 1.23. Cases (a) to (e) are diverging lenses, cases (f) to (k) are converging lenses. Note that all cases, where the curvature of the kink in the potential curve as seen from the zero potential side is concave, are diverging lenses, while those with a convex curvature are converging lenses.

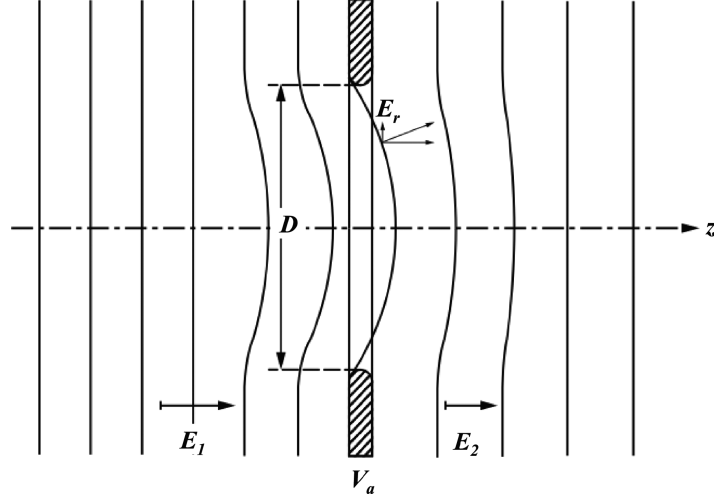


Fig. 1.22. General aperture lens

The transfer matrix of such an aperture is thus (comp. (1.6))

$$\begin{pmatrix} r \\ r' \end{pmatrix}_2 = \begin{pmatrix} 1 & 0 \\ \frac{E_1 - E_2}{4V_a} & 1 \end{pmatrix} \begin{pmatrix} r \\ r' \end{pmatrix}_1. \quad (1.41)$$

The properties of lenses composed of more than one aperture can be calculated by transfer matrix multiplication.

The arrangement shown in Fig. 1.24 can be characterized by the matrix product of the transfer matrices: *first aperture*  $\times$  *uniform field*  $\times$  *second aperture*. The particles have different energies before and behind the arrangement, viz.  $eV_1$  and  $eV_2$ , which is termed an “immersion lens”. This notation is chosen in analogy to light optics, where it characterizes a lens with different indices of refraction in front and behind the lens. The arrangement shown in Fig. 1.25 is characterized by the matrix product of five transfer matrices:

*first aperture*  $\times$  *first uniform field*  $\times$  *second aperture*  $\times$  *second uniform field*  $\times$  *third aperture*.

It represents a so-called einzel lens when the particle energy is the same before and behind the lens,  $eV_3 = eV_1$ .

In this way, the lens properties, such as focal lengths and position of principal planes, can be calculated.

When  $V_3$  is different from  $V_1$ , one has a three-aperture immersion lens (Fig. 1.25). While with a two-aperture immersion lens the focal lengths are fixed for a given  $V_2/V_1$  ratio, a three-aperture immersion lens opens the

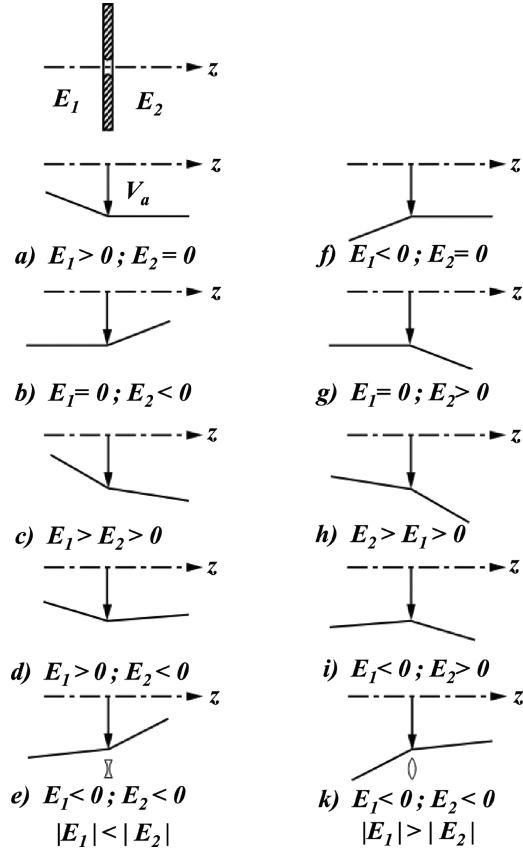


**Fig. 1.23.** Various cases of aperture lenses: (a) to (e) diverging lenses, (f) to (k) converging lenses

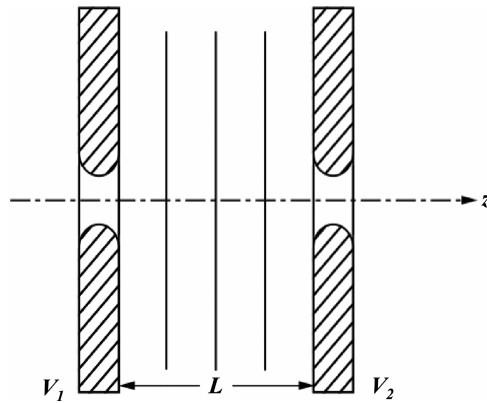


**Fig. 1.24.** Uniform field between two aperture lenses, constituting an “immersion lens”

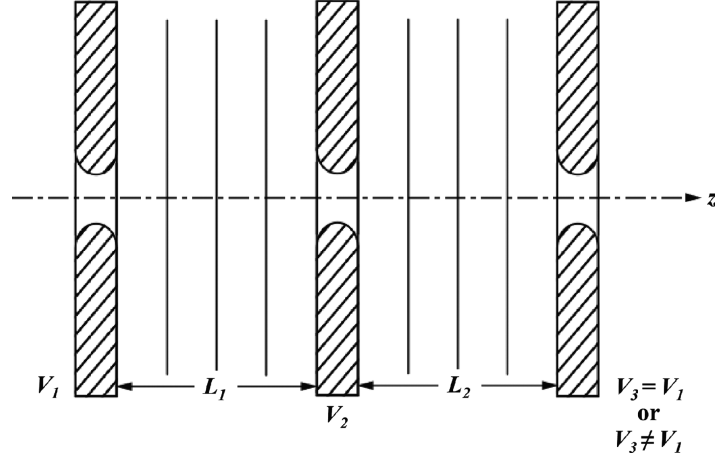


**Fig. 1.25.** Combination of three apertures and two fields constituting an einzel lens ( $V_3 = V_1$ ) or an immersion lens ( $V_3 \neq V_1$ )

possibility of adjusting the focusing action for any ratio  $V_3/V_1$  by varying  $V_2$ . Such lenses are electrostatic “zoom lenses”.

It should be noted that by this simple method of calculating lenses good results are obtained only when the aperture diameters are small in comparison to the distances between the apertures. Otherwise, the fields between the apertures are not uniform and the axial potentials in the aperture differ too much from the potential applied to the aperture electrodes. This restriction for the applicability of (1.40) can be expressed as  $L \ll \Delta V/E$ , which expression should hold for either side of an aperture where a field exists.  $\Delta V$  means the potential difference to either next aperture electrode.

When the above condition is not met, i.e. when the aperture diameter is larger, the formula is still applicable with reasonably good results, when for the  $V_a$  not the potential of the aperture but for the axis point within the aperture is taken. Because of field penetration these two differ the more the larger the aperture diameter is in relation to the distances of the neighboring apertures. This is the case in particular when  $V_a$  has a maximum or a minimum.

### 1.9 Passage of Charged Particles Through an Electrode with Slotted Aperture

When the aperture in an electrode separating spaces of different field strength is not circular but a slot (Fig. 1.26), such that its width



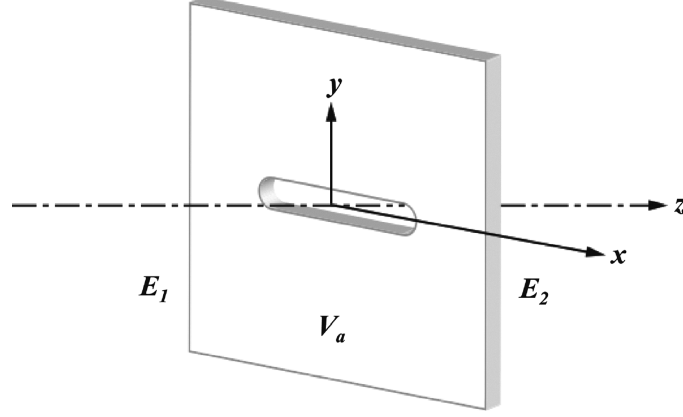


**Fig. 1.26.** Slotted aperture between different fields

( $y$ -direction) is small in comparison to its length ( $x$ -direction), the lens action is only in the  $y$ -direction.

The formula for the focal length (comp. (1.40)) is then

$$f = \frac{2V_a}{E_2 - E_1}. \quad (1.42)$$

The lens action is twice as strong as that of a circular aperture, but occurs only in one azimuthal direction.

In the  $x$ -direction no focusing of the trajectories occurs but only a variation of the incremental change of the refractive index. Parallel trajectories continue being parallel (Fig. 1.27).

In case the particles emitted from a planar surface are accelerated through a slotted electrode (Fig. 1.28), the defocusing by the slot has to be taken into account. Its focal length is (for  $V_1 \ll V_a$ )

$$-f = \frac{2V_a}{E} = 2L. \quad (1.43)$$

The virtual subject located at the distance  $L$  behind the emitting surface is now imaged to the emitting surface itself with the magnification  $r_b/r_a = 1/2$ .

The beam radius at the aperture is of course the same as with a round aperture

$$r_B = r_a + 2L\sqrt{\frac{V_1}{V_a}},$$

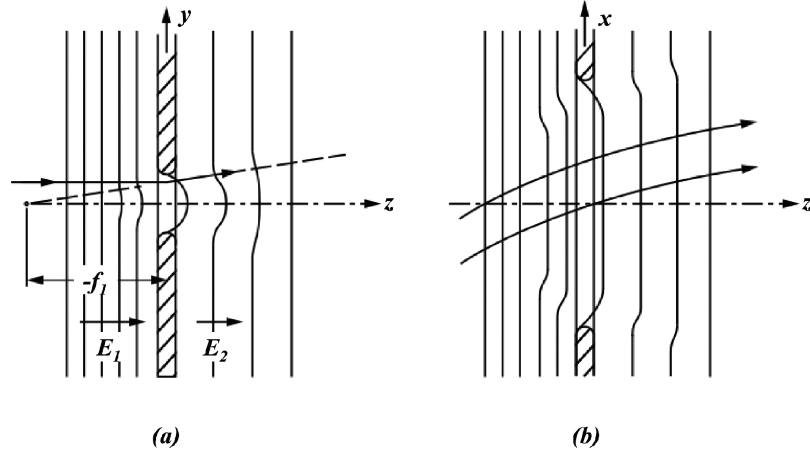


**Fig. 1.27.** Action of slotted aperture between different fields: (a) lens action, (b) bending of trajectories

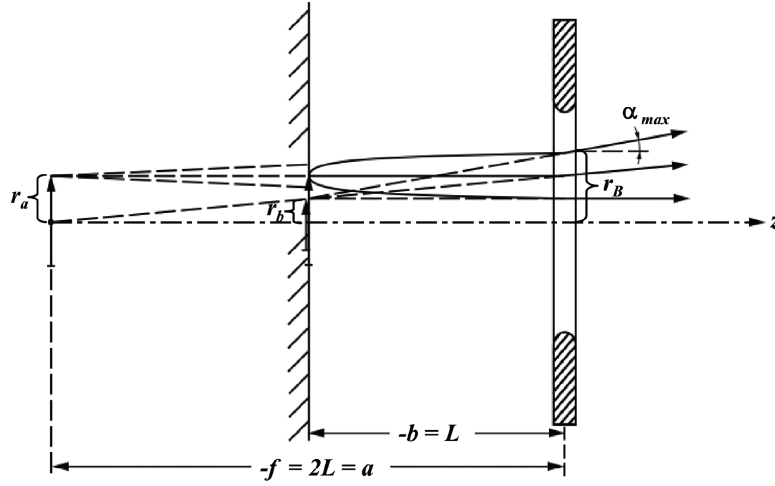


**Fig. 1.28.** Imaging of emitting surface by acceleration field and slotted aperture

but the maximum beam angle in the direction of the lens action is now

$$\alpha_{\max} = \sqrt{\frac{V_1}{V_a}} + \frac{r_B}{2L}.$$

### 1.10 Emission Lenses

The usual requirement in dealing with charged particles emitted from a surface is to form them into a beam with a certain energy and shape,

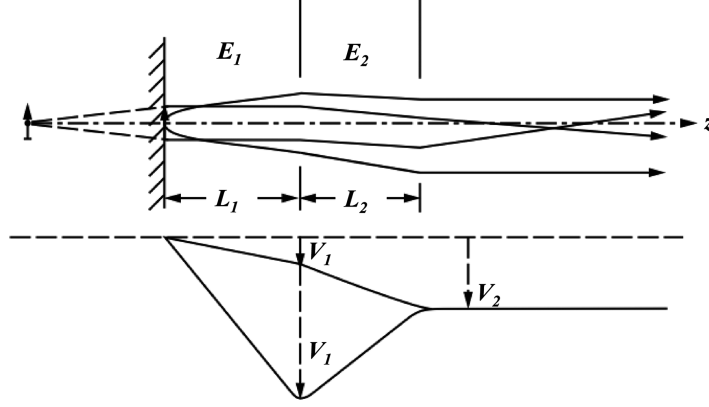


**Fig. 1.29.** Emission lens with two different modes of operation

or to form an image of the surface with them. This is done with an emission lens (for electrons also called cathode lens).

The simplest emission lens is obtained by adding a second apertured electrode to the acceleration electrode (Fig. 1.29).

The two electrodes with their apertures constitute an immersion lens. Together with the uniform acceleration field they form the emission lens. The lens can be treated by multiplying the matrix for the first aperture lens with that of the combination: field along  $L_2$  plus second aperture lens

$$M = \begin{pmatrix} m_{11} & m_{12} \\ m_{21} & m_{22} \end{pmatrix} = \begin{pmatrix} 1 & 0 \\ -\frac{1}{f_1} & 1 \end{pmatrix} \begin{pmatrix} 1 & \frac{2L_2}{\sqrt{V_2/V_1+1}} \\ -\frac{1}{f_2} & \sqrt{\frac{V_1}{V_2}} - \frac{1}{f_2} \frac{2L_2}{\sqrt{V_2/V_1+1}} \end{pmatrix},$$

where the focal lengths  $f_1$  and  $f_2$  of the two apertures are given by

$$-\frac{1}{f_1} = \frac{E_1 - E_2}{4V_1} = \frac{V_1}{4L_1V_1} - \frac{V_2 - V_1}{4L_2V_1} = \frac{1}{4L_1} - \frac{1}{4L_2} \left( \frac{V_2}{V_1} - 1 \right), \quad (1.44)$$

$$-\frac{1}{f_2} = \frac{E_2}{4V_2} = \frac{V_2 - V_1}{4L_2V_2} = \frac{1}{4L_2} \left( 1 - \frac{V_1}{V_2} \right). \quad (1.45)$$

We obtain

$$r_2 = m_{11}r_1 + m_{12}r'_1, \quad (1.46)$$

$$r'_2 = m_{21}r_1 + m_{22}r'_1. \quad (1.47)$$

The matrix coefficients are found to be

$$\begin{aligned}
 m_{11} &= 1 - \frac{1}{f_1} \frac{2L_2}{\sqrt{V_2/V_1} + 1} = 1 - \frac{m_{12}}{f_1}, \\
 m_{12} &= \frac{2L_2}{\sqrt{V_2/V_1} + 1}, \\
 m_{21} &= -\frac{1}{f_2} - \frac{1}{f_1} \left( \sqrt{\frac{V_1}{V_2}} - \frac{1}{f_2} \frac{2L_2}{\sqrt{V_2/V_1} + 1} \right) = -\frac{1}{f_2} - \frac{m_{22}}{f_1}, \\
 m_{22} &= \sqrt{\frac{V_1}{V_2}} - \frac{1}{f_2} \frac{2L_2}{\sqrt{V_2/V_1} + 1} = \sqrt{\frac{V_1}{V_2}} - \frac{m_{12}}{f_2}.
 \end{aligned}$$

Several options are open to shape the beam for given distances  $L_1$  and  $L_2$  by variation of the voltage ratio  $V_1/V_2$ . The value  $eV_2$  is the energy of the beam after passing through the lens.

An important case for beam sources is telescopic imaging (Fig. 1.30), i.e. particles starting from the surface from different points on parallel trajectories travel again on parallel trajectories after acceleration through the emission lens. In particular, particle trajectories starting parallel to the axis are also parallel to the axis after the lens. The angular spread is then entirely due to the initial energy.

The condition for telescopic imaging is that  $r'_2$  be independent of  $r_1$ , or in particular that for  $r'_1 = 0$  also  $r'_2 = 0$ . This is the case for

$$m_{21} = 0. \quad (1.48)$$

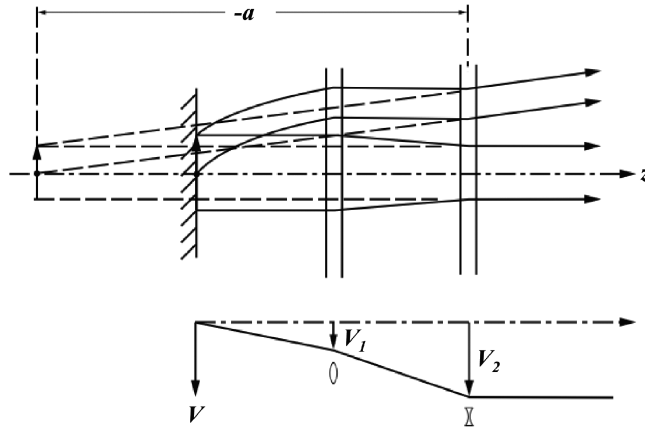


**Fig. 1.30.** Telescopic imaging through emission lens by converging-diverging apertures

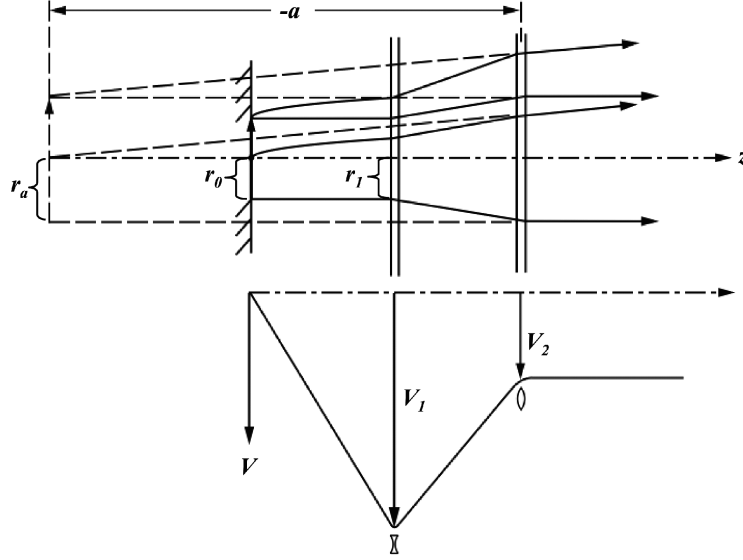


**Fig. 1.31.** Telescopic imaging through emission lens by diverging-converging apertures

The emission lens thus has the focal length

$$f = -1/m_{21} = \infty.$$

There are the two solutions, shown in Figs. 1.30 and 1.31, which can easily be found (with a pocket calculator). For example, with  $L_1 = L_2 = L$ , (1.48) yields  $V_1/V_2 = 0.34$  and  $V_1/V_2 = 2.8$ . The first solution corresponds to Fig. 1.30, where the first aperture acts as a focusing and the second as a defocusing lens. In the second solution (Fig. 1.31) the first aperture is a defocusing lens and the second a focusing one. This is called an accel-decel arrangement because the particles are accelerated in  $L_1$  and decelerated in  $L_2$ . Comparing the two solutions one sees that, for a given final beam energy  $eV_2$ , the field strength in  $L_1$  is much higher in case Fig. 1.31. This can be important when space charge limitations play a role at the emitting surface. There, a higher field strength allows a higher emission current density. On the other hand, for a given beam energy  $eV_2$ , the voltage  $V_1$  required in case Fig. 1.31 may become prohibitively high causing breakdown problems.

Other beam parameters have also to be considered: the position of the virtual emitting surface is found with

$$-a = \left( \frac{r_2}{r_2'} \right)_{r_1=2L_1r_1'} = \frac{2L_1m_{11} + m_{12}}{m_{22}}. \quad (1.49)$$

**Table 1.1.** Telescopic imaging with emission lens after acceleration field ( $L_1 = L_2 = L$ )

$V_1/V_2$	$m_{11}$	$m_{12}/L$	$m_{21}L$	$m_{22}$	$L/f_1$	$L/f_2$	$f/L$	$-a/L$
0.34	0.82	0.74	0	0.70	0.24	-0.17	$\infty$	3.4
2.8	1.51	1.25	0	1.11	-0.41	0.45	$\infty$	3.8

*Note:* These are calculated values for the condition that the aperture diameters are small compared to the aperture distances. This is rarely the case in practice, but by making  $V_1$  adjustable the condition  $f = \infty$  can be met

The virtual object radius  $r_a$  is found (Fig. 1.31) from  $r_1 = r_0$ ,  $r'_1 = 0$  for  $r'_0 = 0$ :

$$r_a = (r_2)_{r'_1=0} = m_{11}r_1, \quad \frac{r_a}{r_0} = m_{11}. \quad (1.50)$$

The maximum beam diameter and aperture angle are obtained with (1.46) and (1.47) by inserting  $r'_{1m} = \sqrt{V_0/V_1}$  (comp. (1.32)),  $r_1 = r_0 + 2L_1r'_{1m}$ :

$$r_{2m} = m_{11}r_0 + (2L_1m_{11} + m_{12})\sqrt{V_0/V_1}, \quad (1.51)$$

$$r'_{2m} = m_{22}\sqrt{V_0/V_1}, \quad (1.52)$$

where  $r_0$  is the radius of the emitting area on the surface.

With the above relations the properties of the emission lens with telescopic imaging are completely described.

The values of the example  $L_1 = L_2 = L$  are compiled in Table 1.1.

Another important application of an emission lens with two apertured electrodes is emission microscopy, where a magnified image of the surface is formed by the emitted particles. The condition for imaging the surface into infinity, in practice to a distance large in comparison with  $L_1$ ,  $L_2$  is that the trajectories starting from the axis point,  $r_0 = 0$ , be parallel to the axis after the emission lens. This yields, with  $r_1 = 2L_1r'_1$ ,

$$\begin{aligned} (r'_2)_{r_0=0} &= m_{21}r_1 + m_{22}r'_1 \\ &= 2L_1m_{21}r'_1 + m_{22}r'_1 = 0, \quad 2L_1m_{21} + m_{22} = 0. \end{aligned} \quad (1.53)$$

Again, there are, for any ratio  $L_1/L_2$ , two solutions  $V_1/V_2$  meeting the above condition (Figs. 1.32 and 1.33). With the same example as above  $L_1 = L_2 = L$ , these solutions are  $V_1/V_2 = 0.18$  and  $V_1/V_2 = 4.5$  [5].

Again, as in telescopic imaging, the second solution represents a large accel-decel voltage ratio, and the same applies as above.

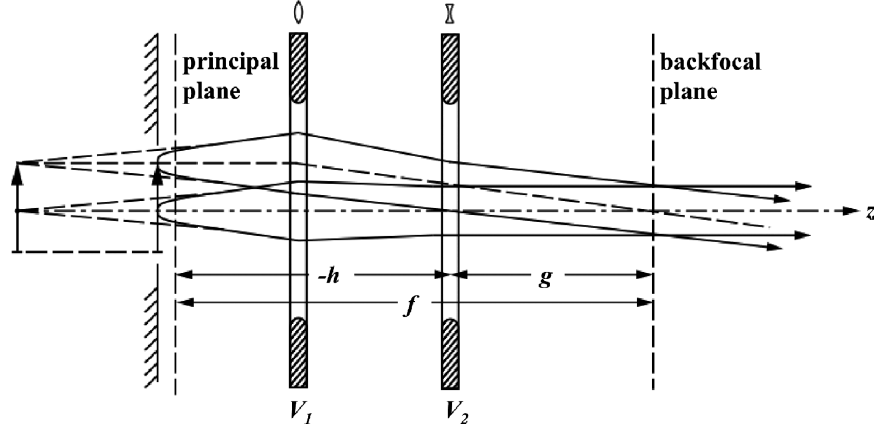


**Fig. 1.32.** Emission microscopy: Imaging of surface to infinity by converging-diverging apertures

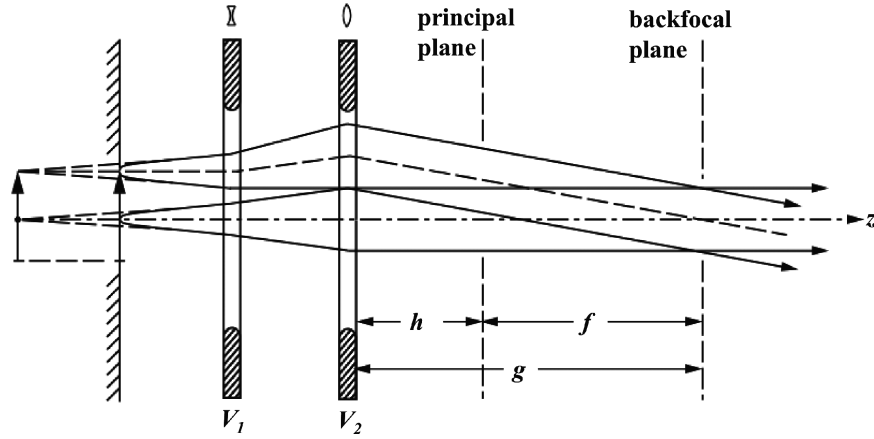


**Fig. 1.33.** Emission microscopy: Imaging of surface to infinity by diverging-converging apertures

The focal length of the emission lens is found from the relation (with  $r_1 = r_0$ ,  $r'_1 = r'_0 = 0$ ).

$$f = \frac{r_0}{r'_2} = -\frac{1}{m_{21}}. \quad (1.54)$$

The backfocal plane is where a trajectory starting with  $r_0 \neq 0$ ,  $r'_0 = 0$  crosses the axis. Its distance from the second electrode of the emission lens is found from (with  $r_1 = r_0$ ,  $r'_1 = r'_0 = 0$ )

$$g = \left( \frac{r_2}{-r'_2} \right)_{r'_0=0} = \frac{m_{11}r_0}{-m_{21}r_0} = -\frac{m_{11}}{m_{21}}. \quad (1.55)$$

**Table 1.2.** Imaging of a planar surface to infinity with a two-aperture emission lens after the acceleration field ( $L_1 = L_2 = L$ )

$V_1/V_2$	$m_{11}$	$m_{12}/L$	$m_{21}L$	$m_{22}$	$L/f_1$	$L/f_2$	$f/L$	$g/L$	$h/L$
0.18	0.47	0.60	-0.28	0.55	0.89	-0.21	3.6	1.7	-1.9
4.5	1.60	1.36	-0.47	0.93	-0.44	0.88	2.1	3.4	1.3

The distance of the principal plane from the second electrode of the emission lens is  $h = g - f$ .

In the backfocal plane all beamlets starting from the individual points on the surface cross the axis. Therefore, the total beam has a waist there, the radius of which is given by

$$r_{2\max} = 2L_1 m_{11} r'_{1m} + m_{12} r'_{1m} = (2L_1 m_{11} + m_{12}) \sqrt{\frac{V_0}{V_1}}. \quad (1.56)$$

It is proportional to  $\sqrt{V_0}$ . When an aperture stop is placed in the backfocal plane eliminating a peripheral part of the beam waist, particles with higher initial energies are discriminated against, viz. those with large initial angles  $\alpha_1$  (see Fig. 1.15). This is generally applied in emission microscopy to improve the lateral resolution, which depends on  $V_0$ .

In practice, the image of the surface is to be formed not in infinity but at some distance  $b$  ( $\gg L_1, L_2$ ). This can be done by making the focal length  $f$  slightly shorter, achievable by adjusting  $V_1/V_2$ , in case Fig. 1.32 to a slightly smaller, in case Fig. 1.33 to a slightly larger value. The magnification is given by the ratio  $M = b/f$ .

Values for the example  $L_1 = L_2 = L$  are listed in Table 1.2.

When a two-electrode emission lens is used for either of the two applications outlined above, the ratio  $V_1/V_2$  is fixed for a given beam energy and given distances  $L_1$  and  $L_2$ . With it also the field strength at the emitting surface,  $E_1 = V_1/L_1$ , is fixed. More flexibility in the operation of an emission lens is obtained when a third aperture electrode is added (Fig. 1.34). This has the advantage that the field strength at the emitting surface can be adjusted to any desired value, within certain limits, and the beam can be accelerated to any final energy  $eV_3$  with adjustable focusing conditions by adjusting the potential  $V_2$  of the second electrode.

The system can be treated as the one above with a transfer matrix. This is obtained by forming the product of the matrix for the lens of Fig. 1.29 with that for Fig. 1.21 and proceeding as outlined above for the two-electrode system. Again, there are in general two solutions, as



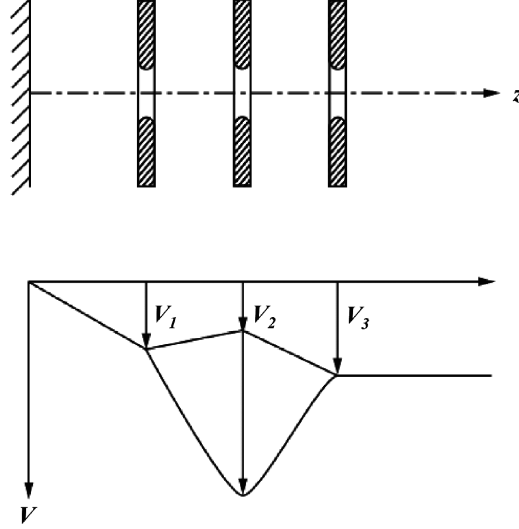


**Fig. 1.34.** Emission lens with three apertures, two operating modes

indicated in Fig. 1.34. When  $V_1 = V_3$ , the three electrodes act as an einzel lens (see below).

The treatment of an optical system with the transfer matrices of uniform fields and aperture lenses is fairly accurate only when the electrodes are planar and parallel and the aperture diameters are small in comparison with electrode distances. In practice this is frequently not the case: The electrodes may have to be conical in order to accommodate some primary radiation (see Fig. 1.35b), and the bores may be larger to reduce lens aberrations. This would correspond to a transition from Fig. 1.35a to b. The axial potential distribution which in Fig. 1.35a is made up of straight portions and sharp kinks, is in Fig. 1.35b a smooth curve with only short near-straight portions and gradual bends. Thus, the lens actions are not sharply localized at the apertures but more widely distributed along the curvatures of the potential curve.

The first-order optical properties of a system are completely determined by the axial potential distribution. This is a consequence of the Laplace equation,  $\text{div } V = 0$  ( $\nabla^2 V = 0$ ), which for rotationally symmetric systems can be written as

$$\frac{\partial^2 V}{\partial r^2} + \frac{1}{r} \frac{\partial V}{\partial r} + \frac{\partial^2 V}{\partial z^2} = 0. \quad (1.57)$$

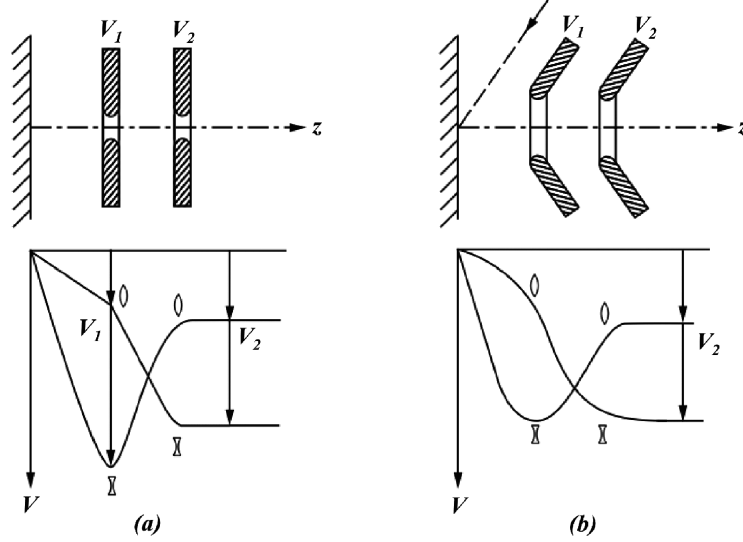


**Fig. 1.35.** Axial potential distributions of two emission lenses with similar optical properties (comp. Fig. 1.23)

When the axial potential distribution  $V(z)_{r=0}$  is given, the paraxial potential distribution is also fixed through (1.57), and with it the paraxial (first order) focusing properties of the system.

Thus, even if the electrodes differ considerably, if the axial potential distribution is similar, so also will be the optical properties of two systems. A great advantage of particle optics compared to light optics is the possibility of continuous variation of optical properties by simple potential variations.

In a triode system such as sketched in Fig. 1.35b with large apertures, the potential  $V_1$  in the case  $V_1 < V_2$  may be adjusted to a very low or even negative value. It is then frequently called “Wehnelt” electrode. The acceleration from the surface is effected mainly by field penetration from the second electrode ( $V_2$ ). This causes a very strong focusing action near the surface such that the beam waist (crossover) occurs within the acceleration field. In such a “gun” the beam crossover serves as a source for further imaging and the “Wehnelt” can be used to control the beam intensity.

### 1.11 Immersion Lenses

The transfer matrix of an immersion lens composed of two planar apertured electrodes has been given already. In the general case there is no

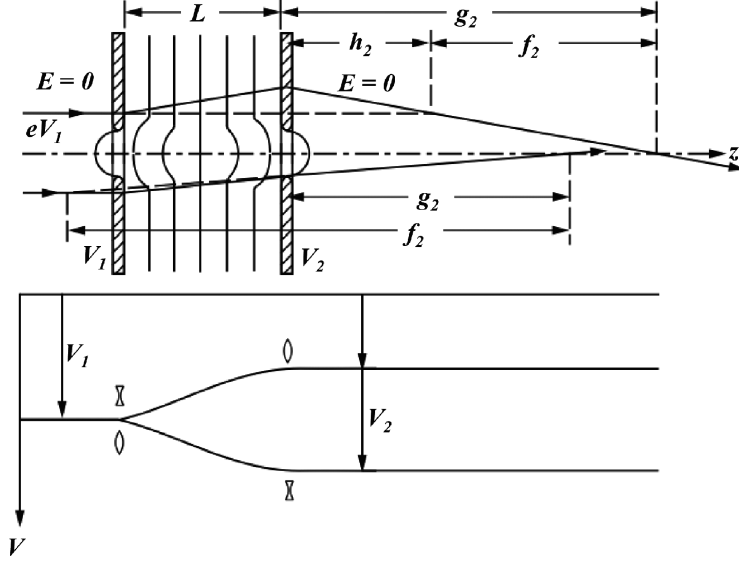


**Fig. 1.36.** Immersion lens with acceleration ( $V_2 > V_1$ ) or deceleration ( $V_2 < V_1$ )

field before the first electrode (Fig. 1.36). The focal length of the first aperture is given by

$$\frac{1}{f_1} = \frac{1}{4L} \left( \frac{V_2}{V_1} - 1 \right). \quad (1.58)$$

The matrix coefficients are the same as given earlier except that  $1/f_1$  is different here.

The two possible cases with acceleration ( $V_2/V_1 > 1$ ) and deceleration ( $V_2/V_1 < 1$ ) are shown in Fig. 1.36. For  $V_2/V_1 = 1$  the matrix coefficients become those for a drift space of length  $L$ .

Focal length  $f_2$  and distance  $g_2$  of the focal plane in the  $V_2$  space are given by

$$f_2 = -1/m_{21}, \quad (1.59)$$

$$g_2 = -m_{11}/m_{21}. \quad (1.60)$$

The distance of the principal plane from the second electrode is

$$h_2 = g_2 - f_2 = \frac{1 - m_{11}}{m_{21}} = \frac{m_{12}}{m_{21}f_1}. \quad (1.61)$$

When (1.59) is carried out, it simplifies to

$$\frac{f_2}{L} = \frac{4 \left( \sqrt{V_2/V_1} + 1 \right)}{V_1/V_2 + V_2/V_1 - 2}. \quad (1.62)$$

Since both  $V_1$  and  $V_2$  have to be positive to let particles pass through the apertures, the focal length  $f$  is always positive for any ratio  $V_1/V_2$  (except the trivial case  $V_2 = V_1$ ). This can be easily verified by inserting some values of  $V_1/V_2$  into (1.62) for either  $V_1/V_2 < 1$  or  $V_1/V_2 > 1$ . Thus, it is not possible to operate such a lens with telescopic imaging as the emission lens shown in Fig. 1.30 (acceleration field plus immersion lens). This means that any change of beam energy is linked with focusing of the beam by the accelerating or decelerating field.

An immersion lens has different focal lengths on the entrance and exit sides. Since in electrostatic optics particle trajectories are reversible, the optical parameters on the entrance side,  $f_1$ ,  $g_1$  and  $h_1$  can be found simply by applying (1.59)–(1.61) with the inverse values of  $V_1/V_2$ . For  $f_1$  follows from (1.62)

$$\frac{f_1}{L} = \frac{4 \left( \sqrt{V_1/V_2} + 1 \right)}{V_2/V_1 + V_1/V_2 - 2}. \quad (1.63)$$

When we form the ratio  $f_2/f_1$  we find with (1.62) and (1.63)

$$\frac{f_2}{f_1} = \sqrt{\frac{V_2}{V_1}}. \quad (1.64)$$

This is a general property of all immersion lenses. It is analogous to immersion lenses in light optics, where  $f_2/f_1 = n_2/n_1$ , the ratio of the refractive indices on both sides.

In practice, immersion lenses are frequently constructed with tubular electrodes (Fig. 1.37). This has the advantage that in comparison with an immersion lens as described above, the lens diameter is smaller for a given beam diameter. Furthermore, as a consequence of the smoother axial potential distribution, the spherical image aberration (aperture aberration) is smaller. The field penetration into the tubes drops to a negligible value at a depth of about the inner tube diameter. Thus, this depth must be kept clear of any constructional elements, which could disturb the field distribution.

The lens properties are determined experimentally or by computation. A variety of lenses with different geometries have been published in tabulated form [6–9].

As is shown in Fig. 1.37, the principal planes are always located on the “slower” side from the end of the lens field. Frequently, particularly with tubular lenses such as shown in Fig. 1.37, they are also interchanged, meaning that the trajectories cross  $P_2$  before  $P_1$ .

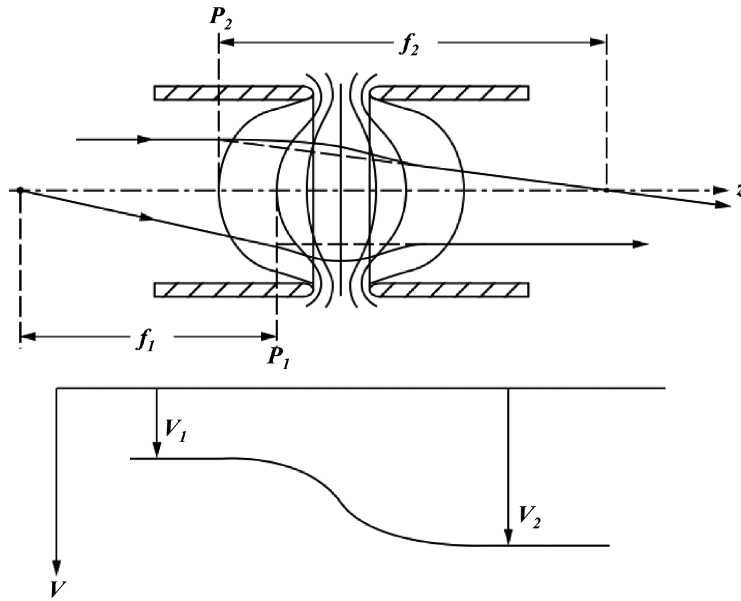


Fig. 1.37. Immersion lens with tubular electrodes

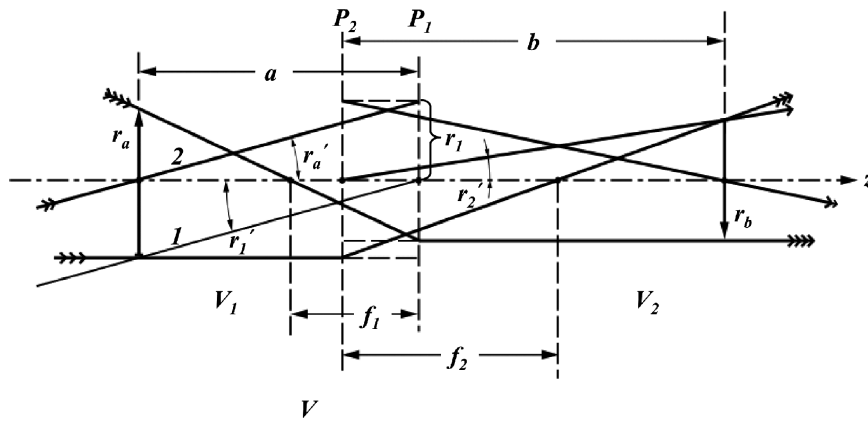


Fig. 1.38. Graphic construction of imaging through immersion lens

When the focal lengths and principal planes are known for a given ratio  $V_1/V_2$  – their position depends on  $V_1/V_2$  – then the imaging properties can be easily found (Fig. 1.38).

Trajectory 1, going through the axis points of  $P_1$  and  $P_2$ , is only refracted:  $r'_2 = r'_1 \sqrt{V_1/V_2}$  (comp. (1.21)). For trajectory 2, passing

through the lens at some distance  $r_1$  from the axis, we have

$$r'_2 = r'_1 \sqrt{\frac{V_1}{V_2}} - \frac{r_1}{f_2}, \quad (1.65)$$

where the first term denotes the refraction and the second the focusing. The equation of trajectory 1 in the  $r$ - $z$  coordinate system ( $V_2$ -space) is thus

$$r(V_2) = r_1 + zr'_2 = r_1 + z \left( r'_1 \sqrt{\frac{V_1}{V_2}} - \frac{r_1}{f_2} \right), \quad (1.66)$$

and with  $r_1 = ar'_1$  ( $a$  = object distance) and  $f_1/f_2 = \sqrt{V_1/V_2}$

$$r(V_2) = r'_1 \left[ a + z \sqrt{\frac{V_1}{V_2}} \left( 1 - \frac{a}{f_1} \right) \right]. \quad (1.67)$$

Trajectory 1 crosses the axis ( $r(V_2) = 0$ ) at the distance  $z = b$ . This inserted in (1.67) yields the imaging equation for immersion lenses

$$\frac{1}{b} + \sqrt{\frac{V_1}{V_2}} \left( \frac{1}{a} - \frac{1}{f_1} \right) = 0. \quad (1.68)$$

The inverse image distance is thus found to be

$$\frac{1}{b} = \sqrt{\frac{V_1}{V_2}} \left( \frac{1}{f_1} - \frac{1}{a} \right) = \frac{1}{f_2} - \frac{1}{a} \sqrt{\frac{V_1}{V_2}}. \quad (1.69)$$

The magnification is found to be (see Fig. 1.38)

$$M = \left| \frac{r_b}{r_a} \right| = \frac{r'_2 b}{r'_1 a} = \frac{b}{a} \sqrt{\frac{V_1}{V_2}}. \quad (1.70)$$

From the figure one can extract the relations

$$\frac{r_a}{a - f_1} = \frac{r_b}{f_1}; \quad \frac{r_b}{b - f_2} = \frac{r_a}{f_2}.$$

This yields

$$\frac{r_a}{r_b} = \frac{a - f_1}{f_1} = \frac{f_2}{b - f_2}$$

and

$$(a - f_1)(b - f_2) = f_1 f_2. \quad (1.71)$$

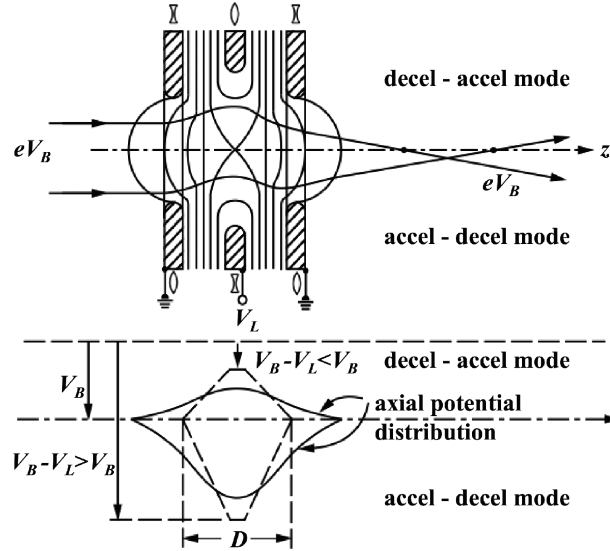


Fig. 1.39. Einzel lens built of three planar apertured electrodes

This is another form of the imaging equation. In light optics it is called Newton's imaging equation. It is equivalent to (1.68) and (1.69).

The above equations are valid not only for two-electrode immersion lenses, but for all lenses with different axial potentials in front and behind. The number of electrodes is arbitrary. Very frequently three-electrode immersion lenses are used. They provide more flexibility because energy change and focusing of the beam can be adjusted independently, within certain limits. They are constructed like einzel lenses (see Fig. 1.39), with the only difference that the first and last electrodes lie on different potentials.

## 1.12 Einzel Lenses

The notation "einzellenses" (einzell=single) is commonly used for three-electrode lenses, where the first and third electrodes are at the same potential. Just as immersion lenses, einzel lenses are always focusing lenses. Fig. 1.39 shows an example of a symmetric einzel lens constructed of apertured electrodes. The potential distribution resembles a saddle surface when the equipotential lines are considered as topographic level lines. Two modes of lens operation are possible: decel-acc and accel-decel, represented by the axial potential distribution shown in the figure. The "lens strength"  $D/f$  of the lens (Fig. 1.40)

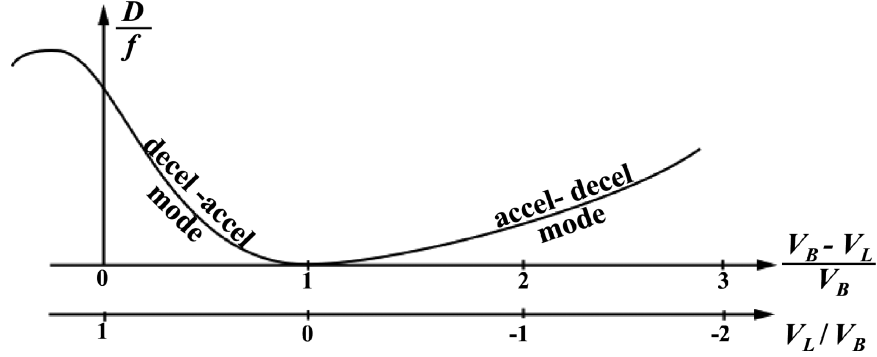


**Fig. 1.40.** Typical dependency of refractive power of einzel lens on the potential of the middle electrode  $V_L$  for a beam energy  $eV_B$

has two branches for the two modes. The decel–accel mode is the one used in most practical applications for two reasons: firstly, since usually the particle source is floating by the acceleration voltage off ground and the two outer electrodes of the lens are grounded, the center electrode is then at a voltage with the same sign as the source voltage and can therefore be supplied via a voltage divider. Secondly, a high refractive power (=short focal length) can be achieved with a center electrode voltage comparable to the source voltage. In the accel–decel mode, a separate voltage supply with the opposite polarity as the source voltage supply is required, and much higher voltages are required for the same refractive power.

In spite of this, the accel–decel mode is advantageous when the focal length required is not too short. The reason is that in this mode both the spherical and the chromatic image aberrations are smaller than in the decel–accel mode. The former is smaller because the trajectories are closer to the axis. The latter because inside the lens field the relative energy spread  $\Delta V/V$  of the particles is smaller. If this mode is chosen, the bore of the center electrode can be made smaller than that of the outer electrodes (Fig. 1.41). This reduces the voltage required for a given focal length.

On the decel–accel branch of the working curve, when the voltage ratio  $V_L/V_B$  is increased to even more positive values, the lens strength  $D/f$  goes through a maximum, i.e. the focal length  $f$  through a minimum. This is the case because with increasing lens strength the focus approaches the lens field. By judicious choice of the lens geometry, this focal length minimum can be made to occur exactly at  $V_L/V_B = 1$



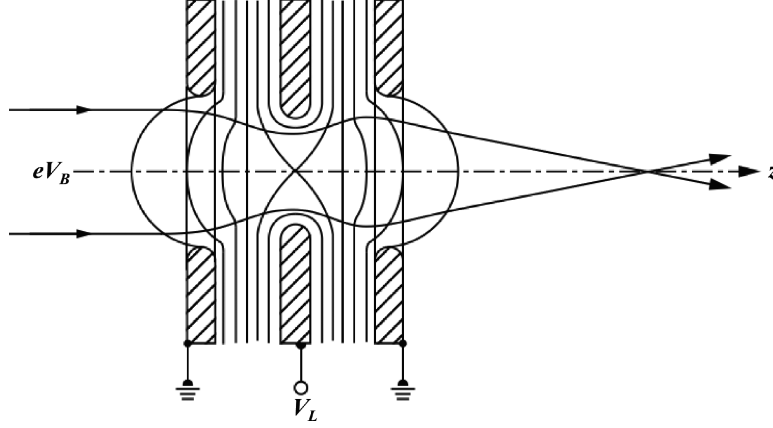


**Fig. 1.41.** Einzel lens geometry advantageous for accel-decel mode

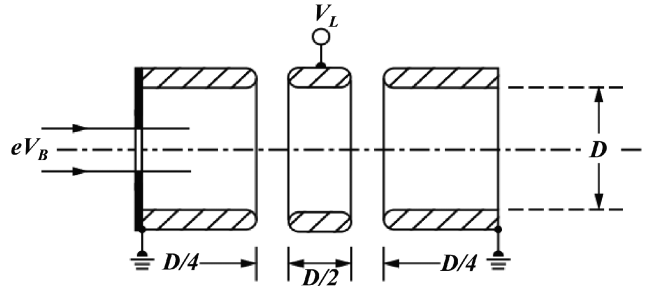


**Fig. 1.42.** Geometry of einzel lens having maximum refractive power with  $V_L = V_B$  (middle electrode at source potential). The focal length is then  $f \approx 2D$ . For  $V_L = 0.5 V_B$  the focal length becomes  $f \approx 10D$

(see Fig. 1.42). For some applications this is advantageous because then both the source and the lens can be supplied by the same voltage.

When the ratio  $V_L/V_B$  is increased beyond +1, there comes a point when the potential of the saddle point equals that of the source, i.e. the particles are slowed down to zero energy, and at a potential slightly above they are reflected. This is one way of switching a beam off.

Figures 1.42–1.45 show examples of various einzel lenses.

In the construction of lenses the most important feature is good concentricity of the lens elements in connection with the necessary electrical insulation to guarantee voltage stability. Distances and contours are less critical as long as everything is rotationally symmetric.

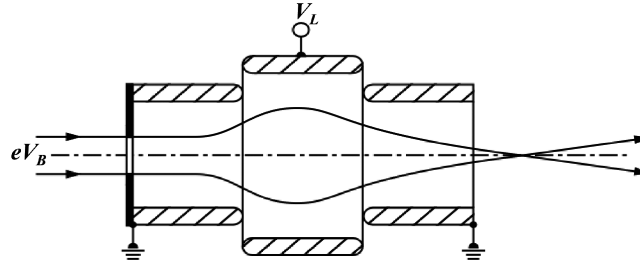


**Fig. 1.43.** Example of einzel lens with decel-accel mode

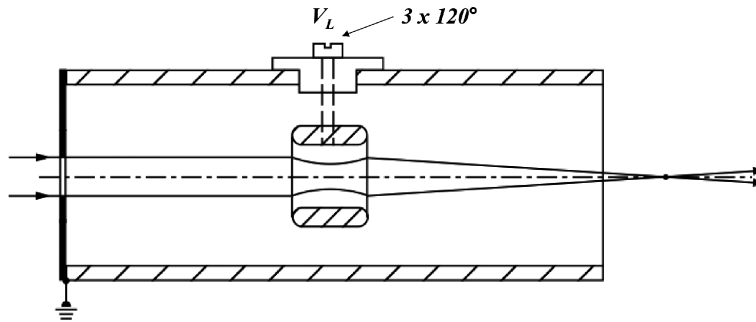


**Fig. 1.44.** Example of einzel lens with accel-decel mode

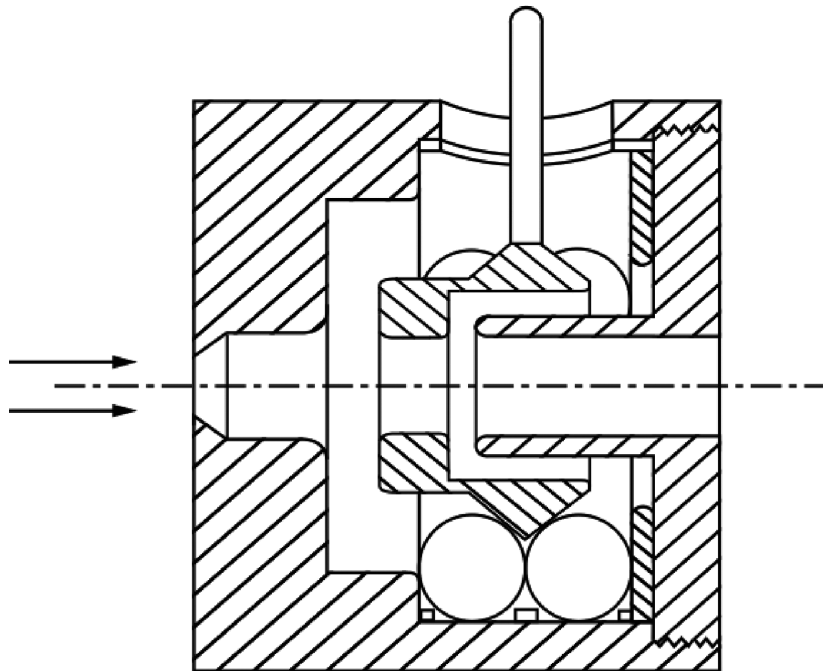


**Fig. 1.45.** Example of einzel lens where the middle electrode is centered and insulated by six precision ceramic balls

Figure 1.45 shows an example of an einzel lens, where the center electrode is held between six high precision sapphire (or alumina) spheres. The lens is self-centering during assembly and the voltage stability is very good because the center electrode touches the centering insulation spheres at six points only. Depending on the application, the electrode contours can be chosen arbitrarily.



<http://www.springer.com/978-3-540-71924-3>

Applied Charged Particle Optics

Liebl, H.

2008, X, 131 p., Hardcover

ISBN: 978-3-540-71924-3